Accepted Manuscript

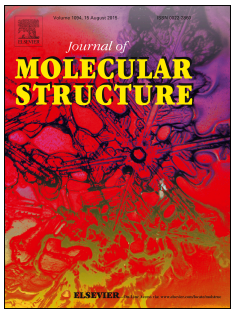

Synthesis, structural characterization, DFT calculations and antiproliferative evaluation of novel spirohydantoin derivatives containing a substituted benzyl moiety

Anita M. Lazić, Lidija D. Radovanović, Bojan Đ. Božić, Biljana Đ. Božić Nedeljković, Vesna D. Vitnik, Željko J. Vitnik, Jelena R. Rogan, Nataša V. Valentić, Gordana S. Ušćumlić, Nemanja P. Trišović

PII: S0022-2860(18)31384-X

DOI: https://doi.org/10.1016/j.molstruc.2018.11.071

Reference: MOLSTR 25900

To appear in: *Journal of Molecular Structure*

Received Date: 6 August 2018

Revised Date: 19 November 2018

Accepted Date: 22 November 2018

Please cite this article as: A.M. Lazić, L.D. Radovanović, Bojan.Đ. Božić, Biljana.Đ. Božić Nedeljković, V.D. Vitnik, Ž.J. Vitnik, J.R. Rogan, Nataš.V. Valentić, G.S. Ušćumlić, N.P. Trišović, Synthesis, structural characterization, DFT calculations and antiproliferative evaluation of novel spirohydantoin derivatives containing a substituted benzyl moiety, *Journal of Molecular Structure* (2018), doi: https://doi.org/10.1016/j.molstruc.2018.11.071.

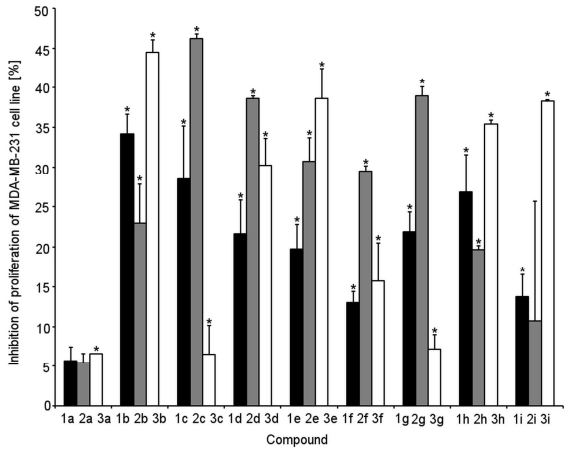

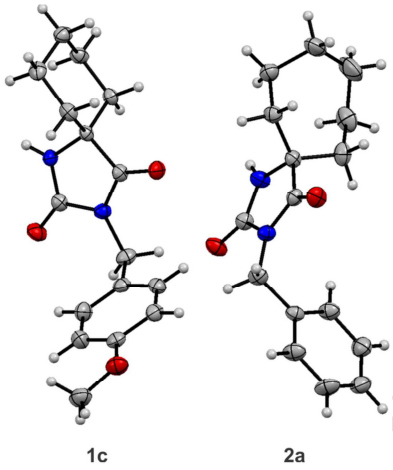

Synthesis, structural characterization, DFT calculations and antiproliferative evaluation of novel spirohydantoin derivatives containing a substituted benzyl moiety

Anita M. Lazić[a], Lidija D. Radovanović[a], Bojan Đ. Božić[b], Biljana Đ. Božić Nedeljković[b], Vesna D. Vitnik[c], Željko J. Vitnik[c], Jelena R. Rogan[d], Nataša V. Valentić[d], Gordana S. Uščumlić[d], Nemanja P. Trišović*,[d]

[a]Innovation Center, Faculty of Technology and Metallurgy, University of Belgrade, Belgrade, Serbia

[b]Faculty of Biology, University of Belgrade, Belgrade, Serbia

[c]Department of Chemistry, Institute of Chemistry, Technology and Metallurgy, University of Belgrade, Belgrade, Serbia

[d]Faculty of Technology and Metallurgy, University of Belgrade, Belgrade, Serbia

*Corresponding author. Tel.: +381113303869; fax: +381113370387.

E-mail address: ntrisovic@tmf.bg.ac.rs

Abstract

Two series of cycloalkanespiro-5-hydantoins, namely cyclohexanespiro-5-hydantoins and cycloheptanespiro-5-hydantoins with a 4-substituted benzyl or a 2-(4-substituted phenyl)-2-oxoethyl group at N3 position, were synthesized and their effects on proliferation of human colon (HCT-116), leukemia (K562) and breast (MDA-MB-231) cancer cell lines were tested. For comparison, we also described the 5,5-diphenylhydantoin analogues. The structural features of the investigated compounds were characterized by elemental analysis, FT-IR, UV-Vis, ^{1}H and ^{13}C NMR spectroscopy and X-ray crystallography. Regarding their structure–activity relationships, it was shown that the substitution on the benzyl moiety with the methoxy, chloro or bromo group potentiated the antiproliferative activity relative to the parent compounds, while an increase in the size of the cycloalkyl group resulted mostly in a decrease of the antiproliferative activity. The single crystal X-ray analysis revealed the existence of dimers and chains formed by the N–H···O hydrogen bonds. The analysis of the molecular descriptors of Lipinski demonstrated that all investigated compounds obeyed the rule of five. To further understand their geometry and electronic structure, DFT calculations with B3LYP method using 6-311++G(d,p) basic set were performed. In this context, the UV-Vis spectra of the investigated compounds were analyzed in detail, whereby the predicted absorption spectra from DFT calculation matched the experimentally obtained ones, with a good correlation. The interesting physico-chemical and pharmacologically relevant properties of the investigated compounds warrant their further investigation.

Keywords: Spirohydantoin; Antiproliferative activity; X-ray structure determination; DFT calculation.

1. Introduction

A number of reasons have been put forward to promote the pharmacological applications of derivatives of hydantoin (imidazolidine-2,4-dione) [1]. These compounds are mostly small molecules, lipophilic and easily penetrate biological membranes. When properly substituted, derivatives of hydantoin exhibit various pharmacological activities, *e.g.* anticonvulsant [2] antiarrhythmic [3], antiviral [4], anti-inflammatory [5] and anti-HIV activity [6]. A representative example of a hydantoin-based drug is phenytoin (5,5-diphenylhydantoin, Dilantin), which is widely used in the control of the *grand mal* types of epilepsy and cardiac arrhythmias [7].

Due to their ability to interfere with multiple signaling pathways influencing cancer metastasis, derivatives of hydantoin have been recognized as promising therapeutic agents in the cancer treatment. The non-steroidal antiandrogen nilutamide (3-(4-nitro-3-trifluoromethylphenyl)-5,5-dimethylhydantoin, Nilandron), is used in combination with surgical castration for the treatment of metastatic prostate cancer [8]. Its ferrocenyl-aryl-hydantoin derivatives have been shown to retain a modest affinity for the androgen receptor, while the *N*-substituted complexes show a weak or moderate antiproliferative effect on hormone-dependent and -independent prostate cancer cells [9]. A linkage of aryl hydantoin-based antiandrogen through a short polyethylene glycol linker to genistein results in a conjugate which derives its antiproliferative activity against prostate cancer cell lines in a similar manner [10].

The 5-benzylidene hydantoin core has also been recognized as a promising scaffold to develop new antiproliferative compounds. Carmi *et al.* have reported that 5-arylidene hydantoins inhibit the EGFR kinase and exhibited an antiproliferative action on A431 human epidermoid carcinoma cells [11]. Regarding the mechanism of action, their growth-inhibitory effects in the lung (A549) cancer cell line has been associated with an accumulation of the cells in the S phase of the cell cycle and induction of genomic DNA damage [12]. *Z*-5-(4-Hydroxyphenyl)methylene hydantoin, a marine natural product, and its derivatives enhance tight junction formation and exhibit anti-invasive and anti-migratory activities *in vitro* against metastatic prostate cancer cells and inhibit tumor growth in distant organs in mouse models [13]. The corresponding structure–activity (SAR) studies have revealed the importance of size and lipophilic parameters, whereby log *P* and molecular volume are the most influential descriptors [14]. Jiang and Zeng have synthesized a series of structurally related hydantoin derivatives and tested for the antitumor activity against HepG2 cancer cells [15].

Spiromustine (3-(2-(bis(2-chloroethyl)amino)ethyl)-1,3-diazaspiro[4.5]decane-2,4-dione) has been developed to cross the blood-brain barrier; thus it has been reported to preferentially localize in brain tumors relative to normal brain tissue [16]. Several diversely substituted diazaspiro hydantoins show growth inhibitory effects against human breast (MCF-7), hepatocellular (HepG-2), cervix (HeLa) and colon (HT-29) cancer cell lines [17]. In this case, substitution at N3 position in the hydantoin ring appears to have a key role in the antiproliferative activity, *i.e.*, compounds bearing the aryl groups show better inhibition relative to those with the alkyl substituents. When additionally investigating the inhibition of the leukemia (K562) cell proliferation, Kavitha *et al.* have reported that the most promising candidate among these compounds induces cell apoptosis through mitochondrial pathway following cell cycle arrest [18]. Hydantoin derivatives of the dihydrothieno[2,3-b]naphtho-4,9-dione system with a distal amine moiety exhibit a similar or greater cytotoxic potency than doxorubicin, a standard chemotherapy drug, against the human breast (MCF-7) and colon (SW 620) cancer cell lines [19]. Their cytotoxicity might be ascribed, among others, to an electrostatic interaction of the positively charged ammonium cation with a negatively charged binding site. Spiro bisheterocycles containing the hydantoin moiety have been shown to promote apoptosis of breast (MCF-7 and MDA-MB-23) cancer cell lines *via* p53-dependent and -independent pathways [20].

Alanazi *et al.* have reported that 5,5-diphenylhydantoins with an alkyl, aryl or phenacyl group at N3 position possess selective activity against the renal (A498 and UO31) cancer cell lines [21]. The introduction of an additional piperydinyl unit has resulted in a compound which shows the strong activity against the melanoma (MDA-MB-435) and breast (MCF-7) cancer cell lines. The docking study has revealed that the hydantoin moiety binds to a narrow hydrophobic pocket in the enzyme through formation of the hydrogen bonds, while the π–π and π–cation interactions between the compound and the binding site have also been observed. In this context, we have shown that 3-(4-substituted benzyl)-5,5-diphenyl- and 3-(4-substituted benzyl)-5-ethyl-5-phenylhydantoins exhibit the superior antiproliferative activity against breast (MDA-MB-231) cancer cell line than against colon (HCT-116) cancer cell line, whereby compounds bearing two phenyl groups at C5 position possess higher potencies than those with one phenyl group [22].

In the present study, two series of cycloalkanespiro-5-hydantoins bearing a 4-substituted benzyl or a 2-(4-substituted phenyl)-2-oxoethyl group at N3 position were synthesized (Figure 1, Series **1** and **2**) and their effects on proliferation of human colon (HCT-116), leukemia (K562) and breast (MDA-MB-231) cancer cell lines were tested. A

focus was thus placed on the overall effects of the structural modifications at N3 and C5 positions of the hydantoin ring on the observed activity. In this context, we described the antiproliferative activities of several key compounds from our previous study [22] and the study of Alanazi [21], 3-(4-substituted benzyl)-5,5-diphenylhydantoins and 3-(2-(4-substituted phenyl)-2-oxoethyl)-5,5-diphenylhydantoins (Fig. 1, Series **3**), against human colon (HCT-116) and breast (MDA-MB-231) cancer cell lines and additionally determined their antiproliferative activities against leukemia (K562) cancer cell line in this study. To understand the geometry and electronic structure of investigated hydantoin derivatives, DFT calculations with B3LYP method using 6-311++G(d,p) basic set were performed. Coupled with the single crystal X-ray analysis of the representative compounds (**1c** and **2a**), the presented study provided basis for understanding of a structure–activity relationship of the investigated compounds, thus enabling development of new synthetic spirohydantoins for the cancer treatment.

<Figure 1>

2. Experimental section

2.1. Chemistry

The ^{1}H and ^{13}C NMR spectral measurements were performed on a Bruker AC 250 spectrometer at 200 MHz for the ^{1}H NMR and 50 MHz for the ^{13}C NMR spectra or on a Bruker 300 spectrometer at 400 MHz for the ^{1}H NMR and 100 MHz for the ^{13}C NMR spectra. The spectra were recorded at room temperature in DMSO-d_6. The chemical shifts were expressed in ppm values referenced to TMS (δ_H = 0 ppm) in ^{1}H NMR spectra, and the residual solvent signal (δ_C = 39.5 ppm) in ^{13}C NMR spectra. FT-IR spectra were recorded using a Bomem MB series 100 spectrophotometer (υ_{max} are given in cm^{-1}) in the form of KBr pellets. The UV-Vis spectra were measured with a Shimadzu 1700 spectrophotometer. The elemental analyses of the investigated compounds were carried out by standard analytical micromethods using an Elemental Vario EL III microanalyzer.

2.1.1. General procedure for the preparation of **1a−1g** and **2a−2g**

The compounds of series **1** and **2** were obtained following the synthetic protocol shown in Scheme 1. 1,3-Diazaspiro[4.5]decane-2,4-dione and 1,3-diazaspiro[4.6]undecane-2,4-dione were synthesized according to the modified procedure of Bucherer and Lieb [23]. The compounds **1a−1i** and **2a−2i** were prepared using a modified procedure described previously [24]. 1,3-Diazaspiro[4.5]decane-2,4-dione or 1,3-diazaspiro[4.6]undecane-2,4-dione (0.01 mol) and potassium carbonate (0.03 mol) were dissolved in DMF (60 cm^3). After half an hour, 4-substituted benzyl halide (0.011 mol) was added in the solution. The reaction mixture was heated at 80 °C for three days. The reaction mixture was poured into three times the volume of water and extracted with ethyl acetate. The organic layer was washed with 5 % sodium hydroxide and water and dried over anhydrous magnesium sulphate. The residual solvent was removed by distillation and the crude product was purified by recrystallization from ethanol.

<Scheme 1>

2.1.2. General procedure for the preparation of **1h, 1i, 2h, 2i, 3h, 3i**

The compounds **1h**, **1i**, **2h**, **2i**, **3h** and **3i** were prepared according to the procedure given in [21] (Scheme 2). A mixture of the appropriate hydantoin (cycloalkanespiro-5-hydantoin or 5,5-diphenylhydantoin) (0.01 mol) and potassium carbonate (0.01 mol) was stirred in acetone (60 cm^3) at room temperature for half an hour. A solution of 1-(4-substituted phenyl)-2-chloroethanone (0.011 mol) in acetone was added and the reaction mixture was stirred for 24 hours at room temperature. The obtained solid was filtered and recrystallized from ethanol.

<Scheme 2>

3-Benzyl-1,3-diazaspiro[4.5]decane-2,4-dione (1a)

Yield 73%; White solid; mp 151−153 °C; FT-IR (KBr pill, ν cm^{-1}) 3323 (NH), 1771, 1708 (C=O); ^{1}H NMR (200 MHz, DMSO−d_6): δ /ppm = 8.81 (s, 1H, NH), 7.33−7.19 (m, 5H, −C_6H_5−), 4.52 (s, 2H, –CH_2–), 1.68−1.26 (m, 10H, −C_6H_{10}−); ^{13}C NMR (50 MHz, DMSO−d_6): δ/ppm = 176.8, 155.9, 137.2, 128.8, 127.6, 127.2, 61.3, 41.0, 38.5, 24.6, 21.0; Elemental anal. calc. (%) for $C_{15}H_{18}N_2O_2$: C, 69.74; H, 7.02; N, 10.84; found: C, 69.70; H, 7.05; N, 10.80.

3-(4-Methylbenzyl)-1,3-diazaspiro[4.5]decane-2,4-dione (1b)

Yield 56%; White solid; mp 211−213 °C; FT-IR (KBr pill, ν cm^{-1}) 3220 (NH), 1771, 1704 (C=O); ^{1}H NMR (200 MHz, DMSO−d_6): δ/ppm = 8.79 (s, 1H, NH), 7.13 (d, *J* = 10 Hz, 2H, −C_6H_4−), 7.08 (d, *J* = 8 Hz, 2H, −C_6H_4−), 4.46 (s, 2H, −CH_2−), 2.26 (s, 3H, −CH_3), 1.66−1.25 (m, 10H, −C_6H_{10}−); ^{13}C NMR (50 MHz, DMSO−d6): δ/ppm = 176.9 155.9, 136.7, 134.2, 129.4, 127.3, 61.3, 40.8, 33.5, 24.4, 21.0, 20.9 (2C); Elemental anal. calc. (%) for $C_{16}H_{20}N_2O_2$: C, 70.56; H ,7.40; N, 10.29; found: C, 70.62; H, 7.42; N, 10.34.

3-(4-Methoxybenzyl)-1,3-diazaspiro[4.5]decane-2,4-dione (1c)

Yield 58%; White solid; mp 162−165 °C; FT-IR (KBr pill, ν cm^{-1}): 3295 (NH), 1773, 1696 (C=O); ^{1}H NMR (200 MHz, DMSO−d_6): δ/ppm = 8.77 (s, 1H, NH), 7.17 (d, 2H, *J* = 8 Hz, −C_6H_4−), 6.89 (d, 2H, *J* = 8 Hz, −C_6H_4−), 4.46 (s, 2H, –CH_2–), 3.73 (s, 3H, −CH_3), 1.62−1.26 (m, 10H, −C_6H_{10}−); ^{13}C NMR (50 MHz, DMSO−d_6): δ/ppm = 176.8, 158.8, 155.9, 129.2, 128.8, 114.1, 61.2, 55.2, 40.5, 33.5, 24.6, 21.00; Elemental anal. calc. (%) for $C_{16}H_{20}N_2O_3$: C, 66.65; H, 6.99; N, 9.72; found: C, 66.76; H, 7.04; N, 9.65.

3-(4-Chlorobenzyl)-1,3-diazaspiro[4.5]decane-2,4-dione (1d)

Yield 66%; White solid mp 185−186° °C; FT-IR (KBr pill, ν cm^{-1}): 3232 (NH), 1773, 1710 (C=O); 1H NMR (200 MHz, DMSO−d_6): δ/ppm = 8.83 (s, 1H, NH), 7.40 (d, *J* = 8 Hz, 2H, −C_6H_4−), 7.24 (d, *J* = 8 Hz, 2H, −C_6H_4−), 4.52 (s, 2H, −CH_2−), 1.68−1.03 (m, 10H, −C_6H_{10}−); ^{13}C NMR (50 MHz, DMSO−d_6): δ/ppm = 176.8, 155.7, 136.1, 132.2, 129.3, 128.8, 61.3, 40.4, 33.5, 24.6, 21.0; Elemental anal. calc. (%) for $C15H_{17}N_2O_2Cl$: C, 61.54; H, 5.85; N, 9.57; found: C, 61.57; H, 5.89; N, 9.52.

3-(4-Bromobenzyl)-1,3-diazaspiro[4.5]decane-2,4-dione (1e)

Yield 70%; White solid; mp 193−194 °C; FT-IR (KBr pill, ν cm^{-1}): 3216 (NH), 1768, 1709 (C=O); ^{1}H NMR (200 MHz, DMSO−d_6): δ/ppm = 8.83 (s, 1H, NH), 7.53 (d, *J* = 10 Hz, 2H, −C_6H_4−), 7.18 (d, *J* = 8 Hz, 2H, −C_6H_4−), 4.50 (s, 2H, −CH_2−), 1.67−1.03 (m, 10H, −C_6H_{10}−); ^{13}C NMR (50 MHz, DMSO−d_6): δ/ppm = 176.8, 155.7, 136.6, 131.7, 129.6, 120.7, 61.3, 40.5, 33.5, 24.6, 21.0; Elemental anal. calc. (%) for $C_{15}H_{17}N_2O_2Br$: C, 53.43; H, 5.08; N, 8.31; found: C, 53.48; H, 5.02; N, 8.35.

3-(4-Cyanobenzyl)-1,3-diazaspiro[4.5]decane-2,4-dione (1f)

Yield 52%; White solid; mp 179−182 °C; FT-IR (KBr pill, ν cm^{-1}): 3243 (NH), 2231 (CN), 1771, 1714 (C=O); ^{1}H NMR (200 MHz, DMSO−*d*6): δ/ppm = 8.88 (s, 1H, NH), 7.81 (d, 2H, *J* = 8 Hz, −C_6H_4−), 7.40 (d, 2H, J = 8 Hz, −C_6H_4−), 4.62 (s, 2H, –CH_2–), 1.70−1.03 (m, 10H, −C_6H_{10}−); ^{13}C NMR (50 MHz, DMSO−d_6): δ/ppm = 176.9, 155.6, 142.7, 132.8, 128.1, 118.9, 110.4, 61.5, 40.7, 33.5, 24.5, 21.0; Elemental anal. calc. (%) for $C_{16}H_{17}N_3O_2$: C, 67.83; H, 6.05; N, 14.83; found: C, 67.90; H, 6.05; N, 14.83.

3-(4-Nitrobenzyl)-1,3-diazaspiro[4.5]decane-2,4-dione (1g)

Yield 74%; Yellowish solid; mp 185−188 °C; FT-IR (KBr pill, ν cm^{-1}): 3235 (NH), 1772, 1708 (C=O); ^{1}H NMR (200 MHz, DMSO−d_6): δ/ppm = 8.90 (s, 1H, NH), 8.21 (d, 2H, *J* = 10 Hz, −C_6H_4−), 7.49 (d, 2H, *J* = 8 Hz, −C_6H_4−), 4.68 (s, 2H, −CH_2–), 1.70−1.03 (m, 10H, −C_6H_{10}−); ^{13}C NMR (50 MHz, DMSO−d_6): δ/ppm = 176.9, 155.6, 147.0, 144.8, 128.4, 124.0, 61.5, 40.6, 33.4, 24.5, 21.0; Elemental anal. calc. (%) for $C_{15}H_{17}N_3O_4$: C, 59.40; H, 5.65; N, 13.85; found: C, 59.32; H, 5.60; N, 13.94.

3-(2-(4-Fluorophenyl)-2-oxoethyl)-1,3-diazaspiro[4.5]decane-2,4-dione (1h)

Yield 40%; White solid; mp 177−180 °C; FT-IR (KBr pill, ν cm^{-1}): 3301 (NH), 1765, 1716, 1701 (C=O); ^{1}H NMR (200 MHz, DMSO−d_6): δ/ppm = 8.85 (s, 1H, NH), 8.13 (q, 2H, *J* = 3.2 Hz, −C_6H_4−), 7.40(t, 2H, *J* = 9 Hz, −C_6H_4−), 4.92 (s, 2H, –CH_2–), 1.79−1.28 (m, 10H, −C_6H_{10}−); ^{13}C NMR (50 MHz, DMSO−d_6): δ/ppm = 191.3, 177.1, 165.8 (d, *J* = 251.5 Hz), 155.9, 131.5 (d, *J* = 9.5 Hz), 131.1 (d, *J* = 2.5 Hz), 116.4 (d, *J* = 22 Hz), 61.7, 44.4, 33.6, 24.6, 21.1; Elemental anal. calc. (%) for $C_{16}H_{17}FN_2O_3$: C, 63.15; H, 5.63; N, 9.21; found: C, 63.04; H, 5.60; N, 9.16.

3-(2-(4-Chlorophenyl)-2-oxoethyl)-1,3-diazaspiro[4.5]decane-2,4-dione (1i)

Yield 45%; White solid; mp 248−250 °C; FT-IR (KBr pill, ν cm^{-1}): 3109 (NH), 1777, 1708, 1697 (C=O); ^{1}H NMR (200 MHz, DMSO−d_6): δ/ppm = 8.85 (s, 1H, NH), 8.05 (d, 2H, *J* = 8 Hz, −C_6H_4−), 7.64 (d, 2H, *J* = 8 Hz, −C_6H_4−), 4.92 (s, 2H, –CH_2–), 1.79−1.29 (m, 10H, −C_6H_{10}−); ^{13}C NMR (50 MHz, DMSO−d_6): δ/ppm) = 191.8, 177.0, 155.6, 139.4, 133.0, 130.3, 129.4, 61.7, 44.4, 33.6, 24.6, 21.0; Elemental anal. calc. (%) for $C_{16}H_{17}N_2O_3Cl$: C, 59.91; H, 5.34; N, 8.73; found: C, 59.87; H, 5.31; N, 8.69.

3-Benzyl-1,3-diazaspiro[4.6]undecane-2,4-dione (2a)

Yield 63%; White solid; mp 117−118 °C; FT-IR (KBr pill, ν cm^{-1}): 3233 (NH), 1771, 1703 (C=O); ^{1}H NMR (200 MHz, DMSO−d_6): δ/ppm = 8.66 (s, 1H, NH), 7.37−7.18 (m, 5H, −C_6H_5−), 4.51 (s, 2H, –CH_2–), 1.86−1.56 (m, 12H, −C_7H_{12}−); ^{13}C NMR (50 MHz, DMSO−d_6): δ/ppm = 178.0, 155.7, 137.2, 128.8, 127.6, 127.2, 63.9, 41.0, 37.2, 28.9, 22.3; Elemental anal. calc. (%) for $C_{16}H_{20}N_2O_2$: C, 70.56; H, 7.40; N, 10.29; found: C, 70.52; H, 7.44; N, 10.26.

3-(4-Methylbenzyl)-1,3-diazaspiro[4.5]decane-2,4-dione (2b)

Yield 56%; White solid; mp 172−175 °C; FT-IR (KBr pill, ν cm^{-1}): 3238 (NH), 1769, 1702 (C=O); ^{1}H NMR (200 MHz, DMSO−d_6): δ/ppm = 8.64 (s, 1H, NH), 7.16 (d, 2H, *J* = 8 Hz, −C_6H_4−), 7.10 (d, 2H, *J* = 8 Hz, −C_6H_4−), 4.46 (s, 2H, −CH_2–), 2.27 (s, 3H, −CH_3), 1.81−1.59 (m, 12H, −C_7H_{12}−); ^{13}C NMR (50 MHz, DMSO−d_6): δ/ppm = 178.0, 155.7, 136.7, 134.2, 129.3, 127.3, 63.8, 40.8, 37.1, 28.9, 22.2, 20.8; Elemental anal. calc. (%) for $C_{17}H_{22}N_2O_2$: C, 71.30; H, 7.74; N, 9.78; found: C, 70.28; H, 7.80; N, 9.75.

3-(4-Methoxybenzyl)-1,3-diazaspiro[4.5]decane-2,4-dione (2c)

Yield 53%; White solid; mp 132−134 °C; FT-IR (KBr pill, ν cm^{-1}): 3259 (NH), 1767, 1706 (C=O); ^{1}H NMR (200 MHz, DMSO−d_6): δ/ppm = 8.61 (s, 1H, NH), 7.15 (d, 2H, *J* = 8 Hz, −C_6H_4−), 6.88 (d, 2H, *J* = 8 Hz, −C_6H_4−), 4.42 (s, 2H, −CH_2−), 3.73 (s, 3H, −CH_3), 1.84−1.57 (m, 12H, −C7H12−); ^{13}C NMR (50 MHz, DMSO−d_6): δ/ppm = 178.0, 158.8, 155.8, 129.2, 128.9, 114.2, 63.8, 55.3, 40.5, 37.15, 28.9, 22.3; Elemental anal. calc. (%) for $C_{17}H_{22}N_2O_3$: C, 67.53; H, 7.33; N, 9.26; found: C, 67.50; H, 7.37; N, 9.23.

3-(4-Chlorobenzyl)-1,3-diazaspiro[4.5]decane-2,4-dione (2d)

Yield 65%; White solid; mp 170−173 °C; FT-IR (KBr pill, ν cm^{-1}): 3231 (NH), 1769, 1721 (C=O); ^{1}H NMR (200 MHz, DMSO−d_6): δ/ppm = 8.68 (s, 1H, NH), 7.39 (d, *J* = 8.4 Hz, 2H, −C_6H_4−), 7.23 (d, *J* = 8.6 Hz, 2H, −C_6H_4−), 4.49 (s, 2H, −CH_2−), 1.85−1.55 (m, 12H, −C7H12−); ^{13}C NMR (50 MHz, DMSO−d_6): δ/ppm = 178.0, 155.6, 136.2, 132.2, 129.3, 128.8, 63.9, 40.4, 37.1, 28.9, 22.3; Elemental anal. calc. (%) for $C_{16}H_{19}N_2O_2Cl$: C, 62.64; H, 6.24; N, 9.13; found: C, 62.59; H, 6.27; N, 9.10.

3-(4-Bromobenzyl)-1,3-diazaspiro[4.5]decane-2,4-dione (2e)

Yield 67%; White solid; mp 178−180 °C; FT-IR (KBr pill, ν cm^{-1}): 3232 (NH), 1770, 1720 (C=O); ^{1}H NMR (200 MHz, DMSO−d_6): δ/ppm = 8.68 (s, 1H, NH), 7.52 (d, *J* = 8.4 Hz, 2H, −C_6H_4−), 7.17 (d, *J* = 8.4 Hz, 2H, −C_6H_4−), 4.47 (s, 2H, −CH_2−), 1.85−1.55 (m, 12H), −C_7H_{12}−); ^{13}C NMR (50 MHz, DMSO−d_6): δ/ppm: 178.0, 155.6, 136.6, 131.7, 129.7, 120.7, 63.9, 40.5, 37.1, 28.9, 22.3; Elemental anal. calc. (%) for $C_{16}H_{19}N_2O_2Br$: C, 54.71; H, 5.45; N, 7.98; found: C, 54.68; H, 5.48; N, 8.03.

3-(4-Cyanobenzyl)-1,3-diazaspiro[4.5]decane-2,4-dione (2f)

Yield 53%; White solid; mp 171−173 °C; FT-IR (KBr pill, ν cm^{-1}): 3239 (NH), 1772, 1720 (C=O); ^{1}H NMR (200 MHz, DMSO−d_6): δ/ppm = 8.73 (s, 1H, NH), 7.81 (d, 2H, *J* = 8 Hz, −C_6H_4−), 7.38 (d, 2H, *J* = 10 Hz, −C_6H_4−), 4.59 (s, 2H, −CH_2–), 1.85−1.56 (m, 12H, −C_7H_{12}−); ^{13}C NMR (50 MHz, DMSO−d_6): δ/ppm: 178.0, 155.5, 142.8, 132.9, 128.2, 118.9, 110.5, 64.1, 40.8, 37.1, 28.9, 22.3; Elemental anal. calc. (%) for $C_{17}H_{19}N_3O_2$: C, 68.67; H, 6.44; N, 14.13; found: C, 68.64; H, 6.49; N, 14.09.

3-(4-Nitrobenzyl)-1,3-diazaspiro[4.5]decane-2,4-dione (2g)

Yield 73%; Yellow solid; mp 166−169 °C; FT-IR (KBr pill, ν cm^{-1}): 3229 (NH), 1772, 1710 (C=O); ^{1}H NMR (200 MHz, DMSO−d_6): δ/ppm = 8.75 (s, 1H, NH), 8.20 (d, 2H, *J* = 10 Hz, −C_6H_4−), 7.47 (d, 2H, *J* = 8 Hz, −C_6H_4−), 4.64 (s, 2H, –CH_2–), 1.86−1.56 (m, 12H, −C_7H_{12}−); ^{13}C NMR (50 MHz, DMSO−d_6): δ/ppm = 178.0, 155.5, 147.1, 144.8, 128.5, 124.1, 64.1, 40.6, 37.1, 28.9, 22.3; Elemental anal. calc. (%) for $C_{16}H_{19}N_3O_4$: C, 60.56; H, 6.03; N, 13.24; found: C, 60.52; H, 6.08; N, 13.20.

3-(2-(4-Fluorophenyl)-2-oxoethyl)-1,3-diazaspiro[4.6]undecane-2,4-dione (2h)

Yield 43%; White solid; mp 140−142 °C; FT-IR (KBr pill, ν cm^{-1}): 3287 (NH), 1769, 1714, 1700 (C=O); ^{1}H NMR (400 MHz, DMSO−d_6): δ/ppm = 8.73 (s, 1H, NH), 8.14 (q, 2H, *J* = 2.8 Hz, −C_6H_4−), 7.42 (t, 2H, *J* = 8.8 Hz, −C_6H_4−), 4.92 (s, 2H, –CH_2–), 1.95−1.59 (m, 12H, −C_7H_{12}−); ^{13}C NMR (100 MHz, DMSO−d_6): δ/ppm = 191.5, 178.4, 166.0 (d, *J* = 255 Hz), 155.7, 131.7 (d, *J* = 9.0 Hz), 131.4 (d, *J* = 2.8 Hz), 116.6 (d, *J* = 22 Hz), 64.5, 37.4, 29.2, 22.2. Elemental anal. calc. (%) for $C_{17}H_{19}N_2O_3F$: C, 64.14; H, 6.02; N, 8.80; found: C, 64.10; H, 6.06; N, 8.77.

3-(2-(4-Chlorophenyl)-2-oxoethyl)-1,3-diazaspiro[4.6]undecane-2,4-dione (2i)

Yield 47%; White solid; mp 206−208 °C; FT-IR (KBr pill, ν cm^{-1}): 3231 (NH), 1775, 1714, 1700 (C=O); ^{1}H NMR (400 MHz, DMSO−d_6): δ/ppm = 8.72 (s, 1H, NH), 8.17−8.10 (m, 2H, −C_6H_4−), 7.46−7.37 (m, 2H, −C_6H_4−), 4.91 (s, 2H, –CH_2–), 1.96−1.59 (m, 12H, −C_7H_{12}−); ^{13}C NMR (100 MHz, DMSO−d_6): δ/ppm = 192.2, 178.4, 155.8, 139.3, 133.2, 130.5, 129.6, 64.5, 44.7, 37.4, 28.9, 22.5. Elemental anal. calc. (%) for $C_{17}H_{19}N_2O_3Cl$: C, 60.99; H, 5.72; N, 8.37; found: C, 60.90; H, 5.76; N, 8.33.

3-(2-(4-Fluorophenyl)-2-oxoethyl-5,5-diphenylimidazolidine-2,4-dione (3h)

Yield 45%; White solid; mp 244−245 °C; FT-IR (KBr pill, ν cm^{-1}): 3233 (NH), 1780, 1704, 1690 (C=O); ^{1}H NMR (400 MHz, DMSO−d_6): δ/ppm = 9.80 (s, 1H, NH), 8.16 (q, 2H, *J* = 3.2 Hz, −C_6H_4−), 7.47−7.37 (m, 12H, 2×C_6H_5 and −C_6H_4−), 5.07 (s, 2H, −CH_2−); ^{13}C NMR (100 MHz, DMSO−d_6): δ/ppm = 191.3, 173.9, 166.1 (d, *J* = 252 Hz), 155.3, 140.0, 131.8 (d, *J* = 9.6 Hz), 131.2 (d, *J* = 2.8 Hz), 129.0, 128.7 , 127.4, 116.6 (d, *J* = 22 Hz), 70.2, 45.3. Elemental anal. calc. (%) for $C_{23}H_{17}N_2O_3F$: C, 71.13; H, 4.41; N, 7.21; found: C, 71.09; H, 4.46; N, 7.18.

3-(2-(4-Chlorophenyl)-2-oxoethyl-diphenylimidazolidine-2,4-dione (3i)

Yield 43%; White solid; mp 241−242 °C; FT-IR (KBr pill, ν cm^{-1}): 3219 (NH), 1780, 1705, 1692 (C=O); ^{1}H NMR (400 MHz, DMSO−d_6): δ/ppm = 9.83 (s, 1H, NH), 8.13 (d, 2H, *J* = 8.4 Hz, −C_6H_4−), 7.71 (d, 2H, *J* = 8.4 Hz, −C_6H_4−), 7.49−7.42 (m, 10H, 2 × C_6H_5), 5.13 (s, 2H, −CH_2−); ^{13}C NMR (100 MHz, DMSO−d_6): δ/ppm = 191.9, 173.8, 155.3, 140.0, 139.7, 133.2, 130.6 , 129.6, 129.0, 128.7, 127.4, 127.1, 126.6, 70.2, 45.4; Elemental anal. calc. (%) for $C_{23}H_{17}N_2O_3Cl$: C, 68.23; H, 4.23; N, 6.92; found: C, 68.20; H, 4.26; N, 6.89.

2.2. Biological characterization

2.2.1. Compounds and solutions

The RPMI 1,640 cell culture medium, fetal bovine serum (FBS), and MTT were purchased from Sigma Chemical Company, USA. MTT was dissolved (5 mg cm^{-3}) in phosphate buffered saline (pH 7.2) and filtered (0.22 lm) before use.

2.2.2. Cells

Normal rat peritoneal macrophages and tumor cell lines including human colon cancer (HCT-116), leukemia (K562) and human breast cancer (MDA-MB-231) cell lines were maintained in a culture using a nutrient medium RPMI 1640 with 10 % FBS and antibiotics.

2.2.3. Treatment of peritoneal macrophages for evaluation of cytotoxic effect

The biocompatibility testing of the newly synthesized compounds is the first step in their biological characterization. The rat peritoneal macrophages were used for the evaluation of biocompatibility. Rat peritoneal macrophages were seeded in 96-well flat-bottomed microtiter plate and cultivated in 0.1 cm^3 of full culture media during 24 h. After that, the investigated compounds were added to cells in the final concentrations (0.01, 0.1, 1, 10, and 100 μmol dm^{-3}), except in the control wells, where only the medium was added. Thusly prepared cell cultures were incubated during an additional 24 h. The stock solutions of the compounds were prepared in DMSO and dissolved in the corresponding medium to the required working concentrations. The effects of the investigated compounds on the viability/proliferation of peritoneal macrophages was determined 24 hours later by the MTT test [25], modified by Ohno and Abe [26]. Briefly, 0.02 cm^3 of MTT dye (5 mg cm^{-3}) was added to each well. After incubation for further 3 h, 0.1 cm^3 of 10 % sodium dodecyl sulfate was added to extract the insoluble product formazan resulting from conversion of the MTT dye by viable cells. The number of viable cells in each well is proportional to the intensity of the absorbance of light, which was then read in an ELISA plate reader at 570 nm.

2.2.4. Treatment of cell lines for antiproliferative *in vitro* screening

The target cells HCT–116 (10000 cells per well), K562 (100000 cells per well) and MDA–MB–231 (100000 cells per well) were seeded in triplicate into a wells of a 96-well, flat-bottomed microtiter plate in 0.1 cm^3 culture medium. Twenty-four hours later, after the cell adaptation and adherence for both cell lines, 0.1 cm^3 of the investigated compound was added to cells in the final concentration (0.01, 0.1, 1, 10 and 100 μmol dm^{-3}), except in the control wells, where only culture medium was added to the cells and was incubated during additional 24 h. The effect of the investigated compounds on cancer cell survival was determined after 24 h by the MTT test described in the previous section. The antiproliferative effect of the compounds was expressed as a percentage of inhibition of proliferation of non-treated cell. It was calculated as 100% minus the ratio between the absorbance of each dose

of the compounds.

2.3. X-ray structure determination

Single-crystal X-ray diffraction data were collected at room temperature (295 K) on an Oxford Gemini S diffractometer equipped with CCD detector using monochromatized Mo *K*α radiation (λ = 0.71073 Å). Intensities were corrected for absorption using the multi-scan method. Both structures were solved by direct methods (SIR92) [27] and refined on F^2 by full-matrix least-squares using the programs SHELXL-97 (**1c**) [28], SHELXL 2018-3 (**2a**) [29] and WinGX [30]. All non-hydrogen atoms were refined anisotropically. The positions of H atoms connected to C atoms in **1c** and to C and N atoms in **2a** were calculated on geometric criteria and refined using the riding model with $U_{iso} = 1.2U_{eq}$(C,N). The hydrogen atom bonded to N1 in **1c** was found in Δ*F* maps and added to the structural models before the final cycle of refinement with the fixed positional and atomic displacement parameters. The selected crystal data and refinement results for **1c** and **2a** are listed in Table 1. The crystallographic data for **1c** and **2a** were deposited at the Cambridge Crystallographic Data Centre with CCDC reference number 1851483 and 1851484.

<Table 1>

2.4. Computational details

All DFT calculations were performed using the Gaussian 09 program package [31] with B3LYP method [33] and 6-311++G(d,p) basis set. The default convergence criteria were used without any constraint on the geometry. The stability of the optimized geometry was confirmed by frequency calculations, which gave real values for all frequencies. The solvent effect was introduced by the Conductor Polarizable Continuum Model (CPCM) [33].

UV absorption energies of these compounds were calculated by TD-DFT B3LYP method in ethanol as solvent. The frontier molecular orbital energies and energy gap of the investigated compounds are also calculated at the same level of DFT theory. The GaussView 5.0 graphical interface was used to visualize molecular orbitals [34].

3. Results and Discussion

3.1 Antiproliferative evaluation

The antiproliferative potential of the investigated compounds was evaluated against HCT-116, K562 and MDA-MB-231 cancer cell lines. The cytotoxicity assays against tumor cell lines were performed *in vitro* with various concentrations of compounds [35]. The results for each compound were reported as the percentage of inhibition of treated cells prolifertion compared to the non-treated control cells. First of all, the *in vitro* screening data have revealed that all investigated compounds are non-toxic to normal cells. On the other side, all investigated compounds demonstrate a statistically significant antiproliferative potential against to different tumor cells in the investigated concentration range.

The investigated compounds exhibit mild to moderate inhibitory effects against proliferation of all three investigated tumor cell lines at concentration of 100 μmol dm^{-3} (Figs. 2–4 and Tables S1–S5 (Electronic Supplementary Information)). Some general conclusions concerning structure–activity relationships of the investigated compounds cannot be simply drawn from the data shown in Figs. 2–4. When the substituent X is the same, the increase in the size of the cycloalkyl group mostly results in decrease of the antiproliferative activity. Exceptions from this trend were largely observed with inhibition of HCT-116 cell proliferation. The parent compounds **1a** and **2a** appear to be the least active ones, while the substitution on the benzyl moiety with the methoxy, chloro or bromo group potentiates the antiproliferative activity. Regarding the inhibition of HCT-116 and K562 tumor cell proliferation, the introduction of the methyl group does not produce an improved antiproliferative activity relative to the parent compounds. Based on this, we may postulate that, in these cases, effects of the electron-rich substituent X (attraction or repulsion) may cause either a tighter interaction or a loosening of the contacts to the amino acid residues in the binding pocket of the protein involved in mediating their antiproliferative action. These impacts alter its function, thus resulting in the increased antiproliferative activity relative to the parent compounds. The replacement of the bridging methylene group with the oxoethyl group can result in compounds with a lower antiproliferative activity. However, some exceptions were identified when analysing the inhibition of K562 cancer cell proliferation of cycloalkanespiro-5-hydantoins.

<Figure 2>

<Figure 3>

<Figure 4>

*3.2. Crystal structures of compounds **1c** and **2a***

Compounds **1c** and **2a** crystallize in monoclinic systems, but in different space groups: $P2_1/c$ for **1c** and $P2_1/n$ for **2a**. The asymmetric units of compounds together with atomic numbering scheme are presented in Fig. 5. The hydantoin and cyclohexane (C5–C10) rings in **1c** are almost perpendicular, with dihedral angle of 89.5(1)°. The analogous angle for the cycloheptane (C5–C11) ring in **2a** is similar and amounts 89.1(1)°. Both cyclohexane and cycloheptane rings adopt a distorted chair conformation and the maximal deviations from their corresponding planes are: 0.256(2) Å for C9 atom in **1c** and 0.382(2) for C7 atom in **2a**. The hydantoin ring in **1c** is more planar than the same ring in **2a**, where maximal deviations are 0.0148(1) Å for N3 and 0.0181(7) Å for C4. The selected bond lengths, angles and torsion angles for both compounds are listed in Table 2. The values are similar with analogous bond lengths, angles and torsion angles found in related hydantoin derivatives [22, 36, 37].

<Figure 5>

The molecules of **1c** are linked by strong intermolecular N–H···O hydrogen bonds (Table 3) between N1 atom, which belongs to the hydantoin ring of one molecule and O2 atom from the hydantoin ring of an adjacent molecule, permitting the formation of infinite pseudo-chains along [010] direction (Fig. 6). The formation of supramolecular chains is not unusual for these compounds and the chains have been found in crystal packing of similar hydantoin derivatives [22]. The neighboring chains are further stabilized by weak C–H···π interactions (H···*Cg* distance is 2.860 Å) between H18 atom from the metoxy group and the adjacent phenyl ring (Fig. 7) and together with numerous C–H···O contacts (Table 3) construct a three-dimensional network.

By intermolecular N–H···O hydrogen bonds (Table 3 and Fig. 8), the molecules of **2a** are connected into centrosymmetric dimmers parallel to the *b*-axis. The formation of the centrosymmetric dimmers are not rare for this type of compounds and they are found in similar systems [22, 36, 37]. The crystal packing of **2a** is stabilized by the C–H···O interactions (Table 3), while additional weak C–H···π interactions (H···Cg distance is 2.940 Å) between H16 atom from one phenyl ring and the π-system of the adjacent phenyl ring (Fig. 9) allow the formation of a three-dimensional structure.

<Table 2>

<Table 3>

<Figure 6>

<Figure 7>

<Figure 8>

<Figure 9>

Both introduction of different substituents X and change in the size of the cycloalkyl group produce a variety in their crystal structures. Despite N–H···O hydrogen bonds dominate, weak interactions promote either stabilization of the crystal structure or its alteration. Regarding compounds **1d** and **1e**, we have previously reported that halogen bonding (X···O) interactions form a supramolecularpseudo-hexagonal network [37]. On the other side, compounds **2d** and **2e** build a different crystal packing based on the X···π interactions. It is clear that tailoring the crystal structure of the investigated compounds through the proposed structural changes should be taken into account when considering their biopharmaceutical aspects, especially those related to their low aqueous solubility. Poorly soluble compounds can provide a risk of low bioavailability with consequences for safety and efficacy. However, a comprehensive knowledge of drugs at the molecular level is required to determine the appropriate approach to improving solubility and dissolution rate.

3.3. Molecular geometry

By applying the DFT method at B3LYP/6-311++G(d,p) level of theory, the optimized geometry parameters for all investigated cycloalkanespiro-5-hydantoines were determined. The most significant geometric parameters (bond lengths, bond angles and torsion angles) are listed in Tables S6 and S7 (Electronic Supplementary Information).

According to the DFT calculations, the cycloheptanespiro-5-hydantoine derivatives exist in two conformational forms relative to each other as 81:19. The first form is presented in Fig. 10, while in the other form the cycloheptane rings occupies a stable conformation of the distorted chair (Fig. S1, Electronic Supplementary Information). The difference in energy between these two conformations is 0.868 kcal mol^{-1}.

<Figure 10>

As expected, the heterocyclic ring is affected by a π-conjugation of the amide type

which is evident from the N–C bond lengths (N1–C2, N1–C5, N3–C2 and N3–C4, Table S6 and S7, Electronic Supplementary Information) [38]. The substituent effect is reflected on small changes of length of bonds bridging the hydantoin and phenyl rings. An increase of the electron accepting ability of the substituent X is associated with a shortening of the N–C11 bond in the compounds of series **1** and the N–C12 bond in the compounds of series **2**, contrary to the case of the electron donating substituents, where a slight lengthening is observed. On the other side, the C11–C12 bond in the compounds of series **1** and the C12–C13 bond in the compounds of series **2** lengthen along with an increase of the electron accepting ability of the substituent X when compared to the parent compounds. The electron donating substituents have an opposite effect. The planes defined by the hydantoin and cycloalkyl rings are approximately perpendicular to each other. The situation is similar regarding the relative orientation of the hydantoin and phenyl rings (Table 2).

When comparing the crystallographically determined structure and structure calculated by the DFT methods, it can be seen that the main differences result from the different bond lengths and bond angles in the cycloalkane ring (the difference ranges from 0.012 to 0.033 A). This can be attributed to so-called packing effects, which distort the structures. Analogously, a notable difference in the length of the N1–C2 and N1–C5 bonds can be ascribed to the involvement of the N1 atom in various intermolecular interactions, primarily hydrogen bonding, which is not present in the isolated state, *i.e.* in the DFT calculations. Furthermore, the differences found in the relative orientation of the hydantoin and lipophilic cycloalkyl and phenyl groups in the crystal and as an isolated molecule indicate that these molecules can easily change their conformation upon binding to a protein.

3.5. Experimental and theoretical study of electronic absorption spectra

The absorption spectra of the investigated compounds retain essentially the character of those of 3-(4-substituted benzyl)-1,3-diazaspiro[4.4]nonane-2,4-diones [36]. Only the absorption spectra of the compounds of series **2** in ethanol are given here (Fig. 11 and Table 4), because both series of compounds (**1** and **2**) exhibit the same trends in λ_{max} as a function of the nature of the substituent X and no significant solvatochromic shift was observed. Their main feature is an intense absorption band with a shoulder on the low-energy side in the region of 207–266 nm and a broad, weak absorption band in the region of 274–281 nm.

<Figure 11>

<Table 4>

When the donating or accepting ability of the substituent X increases, a red shift of the absorption maxima is observed. It is evident that, because of the C,H-hyperconjugation of the bridging CH_2 group, the chromophoric system involves both hydantoin and aryl moieties. To understand the shift of this band under the influence of the substituent X, the data from Table 4 were plotted as a function of the Hammett substituent constant (Fig. 12).

<Figure 12>

There is a split in the Hammett plot at the parent compound, whereby the electron-donating effect is somehow stronger than electron accepting effect (ρ = +12.4 *vs*. ρ = –10.8). When the substituent X is a resonance electron-accepting substituent (NO_2 and CN), the data fall distinctly off the linear relationship, as expected.

The UV-Vis absorption spectra for representative compounds were calculated in relation to their optimized geometry by applying the B3LYP method with 6-311++G(d,p) basic set (Fig. 13, Table S8). Solvent effects were determined using the TD-DFT method.

In the compound **2c** with the electron-donating methoxy group, a closer look into the two major transitions (HOMO→LUMO+2 and HOMO→LUMO+4) based on the shape of the molecular orbital in Fig. 13a suggests a typical $\pi \rightarrow \pi^*$ character. When the substituent X is the electron-accepting NO_2 group (compound **2g**), a higher amount of the orbital distribution is observed on the aryl moiety in the LUMO orbital. Thus, charge may transfer in the HOMO–2→LUMO and HOMO–1→LUMO transitions resulting in the observed absorption bands (Fig. 13b).

<Figure 13>

The orbital distributions of their HOMOs and LUMOs are presented in Fig. 14. The HOMO energy describes the region of a molecule, which can donate electrons during the formation of complexes with proteins involved in mediating its biological effects. On the other hand, the LUMO energy refers to its ability to accept the electrons from proteins [39]. In the case of the parent compounds (**1a** and **2a**) or when X is an electron-donating substituent, the HOMOs mainly involve contributions of π-orbitals of the aryl moiety, while the LUMOs are spread across the entire molecule. The electron-accepting substituent X has

the opposite effect: the HOMOs are distributed over the entire molecule, while the LUMOs are shifted towards the aryl moiety. In the case of the compounds with the bridging oxoethyl group, the HOMOs extend mainly over the hydantoin ring, while the LUMOs are mainly composed of those π orbital from the aryl moiety. The HOMO–LUMO energy gaps are in the range from 4.4 to 6.3 eV (Table 5). The larger HOMO–LUMO energy gaps of the investigated compounds refer to their higher kinetic stability and lower chemical reactivity. In comparison with the parent compounds, the electron-donating substituents X elevate both HOMO and LUMO energy levels simultaneously. Oppositely, the HOMO and LUMO energy levels are lower than that of the parent compounds, when X is a resonance electron-accepting substituent (NO_2 and CN). With enlarging the cycloalkane ring, the energy gap remains almost unchanged.

<Figure 14>

<Table 5>

3.6 *'Rule of five' properties*

The Lipinski rule of five is widely used to estimate drug-like properties [40]. According to this rule, compounds with good permeability have log P < 5, molecular weight < 500 g mol^{-1}, the number of hydrogen bond acceptors < 10 and the number of hydrogen bond donors < 5.

The analysis of molecular descriptors shows that the investigated compounds obey rule of five (Table 5). When compared to the phenytoin derivatives [22], the physico-chemical properties of the investigated compounds are moving towards somewhat lower molecular weight (258–335), and coincidentally also somewhat lower lipophilicity (2.6–3.8). As expected, lipophilicity increases with the size of the cycloalkyl group. With the exception of the methoxy group, the introduction of the substituent X results in the increase of lipophilicity relative to the parent compounds (**1a** and **2a**). This will lead to their higher partitioning into the lipophilic phase of a biological membrane or lipophilic domains of a protein. Furthermore, a higher local concentration of the investigated compounds can be expected near a binding site, but it does not necessarily indicate its higher biological activity. On the other side, lipophilicity decreases when the bridging methyl group is replaced with the ethyloxo group. The investigated compounds contain both proton acceptor and proton donor groups, which indicates their high capacity for hydrogen bonding, especially toward proton donor of the binding site. The number of rotatable bonds in the investigated

compounds is almost constant and low, thus indicating that large changes of their conformation upon binding to a binding site are not expected. An increase in polar surface area (PSA) of the investigated compounds arises from both introduction of the substituent X and replacement of the bridging methyl group with the ethyloxo group. Generally, relatively high values of PSA may result in worsening of their absorption.

<**Table 6**>

4. Conclusion

In the present paper, we reported the synthesis and antiproliferative evaluation of two series cycloalkanespiro-5-hydantoins with a 4-substituted benzyl or a 2-(4-substituted phenyl)-2-oxoethyl group at N3 position. For comparison, we also described the 5,5-diphenylhydantoin analogues. The investigated compounds exhibited mild to moderate effects against proliferation of human colon (HCT-116), leukemia (K562) and breast (MDA-MB-231) cancer cell lines at concentration of 100 μmol dm^{-3}, while they were non-toxic to normal cells. Some interesting structure–activity findings were revealed. The substitution on the benzyl moiety with the methoxy, chloro or bromo group potentiated the antiproliferative activity relative to the parent compounds, while an increase in the size of the cycloalkyl group resulted in a decrease in the antiproliferative activity in most cases. The replacement of the bridging methylene group with the oxoethyl group can result in compounds with a lower antiproliferative activity. The investigated compounds were compatible with the ’rule of five’ indicating that they have satisfactory pharmacokinetic properties and bioavailability.

Regarding the crystallographic analysis, the investigated compounds adopted different packing arrangements, either hydrogen bonded dimeric units or one-dimensional pseudo-chains. Controlling the crystal structure of the investigated compounds through the proposed structural changes should be taken into account when considering their biopharmaceutical aspects, especially those related to their low aqueous solubility. The theoretical calculations reproduced the experimental data well, thus describing the geometry and electronic structures accurately and providing detailed spectroscopic results.

We find that the presented results shed light on the strategy for development of new cycloalkanespiro-5-hydantoins with specific physico-chemical properties and antiproliferative activities.

Acknowledgement

The authors are grateful to the Ministry of Education, Science and Technological Development of the Republic of Serbia for financial support (Projects No. 172013, 172035, 173052 and III45007).

References

[1] L. Konnert, F. Lamaty, J. Martinez, E. Colacino, Recent advances in the synthesis of hydantoins: the state of the art of a valuable scaffold, Chem. Rev. 117 (2017) 13757–13809. https://doi.org/ 10.1021/acs.chemrev.7b00067

[2] J.H. Block, J.J.M. Beale, Wilson and Gisvold's textbook of organic medicinal and pharmaceutical chemistry, 11th edn. Lippincott Williams and Wilkins, Philadelphia, 2004, p. 504–505.

[3] A. Czopek, H. Byrtus, A. Zagórska, A. Siwek, G. Kazek, M. Bednarski M, J. Sapa, M. Pawłowski, Design, synthesis, anticonvulsant, and antiarrhythmic properties of novel *N*-Mannich base and amide derivatives of β-tetralinohydantoin, Pharmacol. Rep. 68 (2016) 886–893. https://doi.org/ 10.1016/j.pharep.2016.04.018

[4] A. Tijsma, H.J. Thibaut, D. Franco, K. Dallmeier, J. Neyts, Hydantoin: the mechanism of its *in vitro* anti-enterovirus activity revisited, Antivir. Res. 133 (2016) 106–109. https://doi.org/ 10. 1016 /j. anti viral.2016.07.023

[5] H. Lu, D. Kong, B. Wu, Y. Wang Y, Synthesis and evaluation of anti-Inflammatory and antitussive activity of hydantoin derivatives, Lett. Drug. Des. Discov. 9 (2012) 638–642. https://doi.org/ 10.2174/157018012800673092

[6] R.N. Comber, R.C. Reynolds, J.D. Friedrich, R.A. Manguikian, R.W. Buckheit Jr, J.W. Truss, W.M. Shannon, J.A. Secrist III, 5,5-Disubstituted hydantoins: synthesis and anti-HIV activity, J. Med. Chem. 35 (1992) 3567−3572. https://doi.org/ 10.1021/jm00097a014

[7] T.L. Lemke, D.A. Williams, Foye's principles of medicinal chemistry, 6th edn. Lippincott Williams and Wilkins, Philadelphia, 2008, p. 529.

[8] G.A. Dijkman, R.A. Janknegt, T.M. de Reijke, F.M.J. Debruyne, Long-term efficacy and safety of nilutamide plus castration in advanced prostate cancer, and the significance of early prostate specific antigen normalization, J. Urol. 158 (1997) 160–163. https://doi.org/10.1097/00005392-19970700 0-00051

[9] O. Payen, S. Top, A. Vessières, E. Brulé, M.A. Plamont, M.J. McGlinchey, H. Müller-Bunz, G. Jaouen, Synthesis and structure–activity relationships of the first ferrocenyl-aryl-hydantoin derivatives of the nonsteroidal antiandrogen nilutamide, J. Med. Chem. 51 (2008)

1791–1799. https://doi.org/10.1021/jm701264d

[10] A. George, I. Raji, B. Cinar, O. Kucuk, A.K. Oyelere, Design, synthesis and biological assessment of *N*-adamantyl, substituted adamantyl and noradamantyl phalimidines for nitrite, TNF-α and angiogenesis inhibitory activities, Bioorg. Med. Chem. 26 (2018) 1481–1487. https://doi.org/10.1016/ j.bmc. 2018.01.009.

[11] C. Carmi, A. Cavazzoni, V. Zuliani, A. Lodola, F. Bordi, P.V. Plazzi, R.R. Alfieri, P.G. Petronini, M. Mor, 5-Benzylidene-hydantoins as new EGFR inhibitors with antiproliferative activity, Bioorg. Med. Chem. Lett. 16 (2006) 4021–4025. https://doi.org/10.1016/j.bmcl.2006.05.010

[12] A. Cavazzoni, R.R. Alfieri, C. Carmi, V. Zuliani, M. Galetti, C. Fumarola, R. Frazzi, M. Bonelli, F. Bordi, A. Lodola, M. Mor, P.G. Petronini, Dual mechanisms of action of the 5-benzylidene-hydantoin UPR1024 on lung cancer cell lines, Mol. Cancer. Ther. 7 (2008) 361–370. https://doi.org/10.1158/1535-71 63.MCT-07-0477

[13] A.A. Sallam, M.M. Mohyeldin, A.I. Foudah, M.R. Akl, S. Nazzal, S.A. Meyer, Y.Y. Liu, K.A. El Sayed, Marine natural products-inspired phenylmethylene hydantoins with potent *in vitro* and *in vivo* antitumor activities *via* suppression of Brk and FAK signaling, Org. Biomol. Chem. 12 (2014) 5295–5303. https://doi.org/10.1039/C4OB00553H

[14] M.M. Khanfar, K.A. El Sayed, Phenylmethylene hydantoins as prostate cancer invasion and migration inhibitors. CoMFA approach and QSAR analysis, Eur. J. Med. Chem. 45 (2010) 5397–5405. https://doi.org/10.1016/j.ejmech.2010.08.066

[15] L. Jiang, B. Zeng, Derivatives of hydantoin: synthesis and antiproliferative activity on HepG2 cancer cell line, Adv. Mat. Res. 893 (2014) 512–515. https://doi.org/ 10.4028/ www.scientific. net / AMR.893.512

[16] R. Pazdur, B.G. Redman, T. Corbett, M. Phillips, L.H. Baker, Phase I trial of spiromustine (NSC 172112) and evaluation of toxicity and schedule in a murine model, Cancer. Res. 47 (1987) 4213–4217. http://cancerres.aacrjournals.org/content/47/15/4213

[17] C.S.A. Kumar, S.B.B. Prasad, K. Vinaya, S. Chandrappa, N.R. Thimmegowda, K.S. Rangappa, S. Swarup, Synthesis and antiproliferative activity of substituted diazaspiro hydantoins: a structure-activity relationship study, Invest. New Drugs 27 (2009) 131–139. https://doi.org/10.1007/s10637-008-9150-3

[18] C.V. Kavitha, M. Nambiar, P.B. Narayanaswamy, E. Thomas, U. Rathore, C.S.A. Kumar, B. Choudhary, K.S. Rangappa, S.C. Raghavan SC, Propyl-2-(8-(3,4-difluorobenzyl)-2,5-dioxo-8-azaspiro[bicy- clo[3.2.1]octane-3,4-imidazolidine]-1-yl) acetate induces apoptosis in human leukemia cells through mitochondrial pathway following cell

cycle arrest, PLoS One 8 (2013) e69103. https:// doi.org/ 10.1371/journal.pone.0069103

[19] I. Gomez-Monterrey, G. Santelli, P. Campiglia, D. Califano, F. Falasconi, C. Pisano, L. Vesci, T. Lama, P. Grieco, E. Novellino, Synthesis and cyntotoxic evaluation of novel spirohydantoin derivatives of the dihydrothieno[2,3-*b*]naphtho-4,9-dione systems, J. Med. Chem. 48 (2005) 1152–1157. https:// doi. org/10.1021/jm0408565

[20] L.H. Ramadani, O. Talhi, N. Taibi, L. Delort, C. Decombat, A. Silva, K. Bachari, M.P. Vasson, F. Caldefie-Chezet, Effects of spiro-bisheterocycles on proliferation and apoptosis in human breast cancer cell lines, Anticancer. Res. 36 (2016) 6399–6408. https:// doi. org/10.21873/anticanres.11237

[21] A.M. Alanazi, A.S. El-Azab, I.A. Al-Swaidan, A.R. Maarouf, E.R. El-Bendary, M.A.A. El-Enin, A.A.M. Abdel-Aziz, Synthesis, single-crystal, *in vitro* antitumor evaluation and molecular docking of 3-substituted 5,5-diphenylimidazolidine-2,4-dione derivatives, Med. Chem. Res. 22 (2013) 6129–6142. https:// doi. org/ 10.1007/s00044-013-0597-1

[22] S. Hmuda, N. Trišović, J. Rogan, D. Poleti, Ž. Vitnik, V. Vitnik, N. Valentić, B. Božić, G. Uščumlić, New derivatives of hydantoin as potential antiproliferative agents: biological and structural characterization in combination with quantum chemical calculations, Monatsh. Chem. 145 (2014) 821–833. https://doi. org/10.1007/s00706-013-1149-6

[23] E. Naydenova, N. Pencheva, J. Popova, N. Stoyanov, M. Lazarova, B. Aleksiev, Aminoderivatives of cycloalkanespirohydantoins: synthesis and biological activity, Farmaco 57 (2002)189–194. https://doi.org/10.1016/S0014-827X(01)01198-3

[24] H. Suzuki, M.B. Kneller, D.A. Rock, J.P. Jones, W.F. Trager, A.E. Rettie, Active-site characteristics of CYP2C19 and CYP2C9 probed with hydantoin and barbiturate inhibitors, Arch. Biochem. Biophys. 429 (2004) 1–15. https://doi.org/10.1016/j.abb.2004.05.015

[25] T. Mosmann, Rapid colorimetric assay for cellular growth and survival: application to proliferation and cytotoxicity assays, J. Immunol. Methods. 65 (1983) 55–63. https://doi.org /10.1016/0022-1759(83)90303-4

[26] M. Ohno, T. Abe, Rapid colorimetric assay for the quantification of leukemia inhibitory factor (LIF) and interleukin-6 (IL-6), J. Immunol. Methods. 145 (1991) 199–203. https://doi.org /10.1016/0022-1759(91)90327-C

[27] A. Altomare, G. Cascarano, C. Giacovazzo, A. Guagliardi, Completion and refinement of crystal structures with SIR92, J. Appl. Cryst. 26 (1993) 343–350. https://doi.org/10.1107/S0021889892010331

[28] G.M. Sheldrick, A short history of SHELX, Acta. Cryst. A64 (2008) 112–122. https://doi.org/10.1107/S0108767307043930

[29] G. M. Sheldrick GM, Crystal structure refinement with SHELXL, Acta. Cryst. C71 https://doi.org/10.1107/S2053229614024218 (2015) 3–8.

[30] L.J. Farrugia, WinGX and ORTEP for Windows: an update, J. Appl. Cryst. 45 (2012) 849–854. https://doi.org/10.1107/S0021889812029111

[31] M.J. Frisch, G.W. Trucks, H.B. Schlegel, G.E. Scuseria, M.A. Robb, J.R. Cheeseman, G Scalmani, V Barone, B Mennucci, G.A. Petersson, H. Nakatsuji, M. Caricato, X. Li, H.P. Hratchian, A.F. Izmaylov, J. Bloino, G. Zheng, J.L. Sonnenberg, M. Hada, M. Ehara, K. Toyota, R. Fukuda, J. Hasegawa, M. Ishida, T. Nakajima, Y. Honda, O. Kitao, H. Nakai, T. Vreven, J.A. Montgomery, J.E. Peralta, F. Ogliaro, M. Bearpark, J.J. Heyd, E. Brothers, K.N. Kudin, V.N. Staroverov, T. Keith, R. Kobayashi, J. Normand, K. Raghavachari, A. Rendell, J.C. Burant, S.S. Iyengar, J. Tomasi, M. Cossi, N. Rega, J.M. Millam, M. Klene, J.E. Knox, J.B. Cross, V. Bakken, C. Adamo, J. Jaramillo, R. Gomperts, R.E. Stratmann, O. Yazyev, A.J. Austin, R. Cammi, C. Pomelli, J.W. Ochterski, R.L. Martin, K. Morokuma, V.G. Zakrzewski, G.A. Voth, P. Salvador, J.J. Dannenberg, S. Dapprich, A.D. Daniels, O. Farkas, J.B. Foresman, J.V. Ortiz, J. Cioslowski, D.J. Fox, Gaussian 09, revision C.01.Gaussian, Inc., Wallingford, 2010.

[32] A.D. Becke, Density-functional thermochemistry. III. The role of exact exchange, J. Chem. Phys. 98 (1993) 5648–5652. https://doi.org/10.1063/1.464913

[33] M. Cossi, N. Rega, G. Scalmani, V. Barone, Energies, structures, and electronic properties of molecules in solution with the C-PCM solvation model, J. Comput. Chem. 24 (2003) 669–681. https://doi.org/10.1002/jcc.10189

[34] R. Dennington, T. Keith, J. Millam, GaussView, Version 5.0.9. Shawnee Mission, KS: Semichem Inc., 2009.

[35] I.P. Ejidike, P.A. Ajibade, Ruthenium(III) complexes of heterocyclic tridentate (ONN) Schiff base: Synthesis, characterization and its biological properties as an antiradical and antiproliferative agent, Int. J. Mol. Sci. 17 (2016) 60. https://doi: 10.3390/ijms17010060".

[36] A. Lazić, B. Božić, V. Vitnik, Ž. Vitnik, J. Rogan, L. Radovanović, N. Valentić, G. Uščumlić, Structure-property relationship of 3-(4-substituted benzyl)-1,3-diazaspiro[4.4]nonane-2,4-diones as new potentional anticonvulsant agents. An experimental and theoretical study, J. Mol. Struct. 1127 (2017) 88–98. https://doi. org/10.1016/j.molstruc.2016.07.069

[37] A. Lazić, N. Trišović, L. Radovanović, J. Rogan, D. Poleti, Ž. Vitnik, V. Vitnik, G. Uščumlić, Towards understanding intermolecular interactions in hydantoin derivatives: case of cycloalkane-5-spirohydantoins tethered with a halogenated benzyl moiety, Cryst. Eng.

Comm. 19 (2017) 469–483. https://doi. org/10.1039/C6CE02210C

[38] A. Bakalova, B. Nikolova-Mladenova, R. Buyukliev, E. Cherneva, G. Momekov, D. Ivanov, Synthesis, DFT calculations and characterisation of new mixed Pt(II) complexes with 3-thiolanespiro-5'-hydantoin and 4-thio-1*H*-tetrahydropyranspiro-5'-hydantoin, Chem. Pap. 70 (2016) 93–100. https://doi. org/10.1515/chempap-2015-0194

[39] H.N. Banavath, O.P. Sharma, M.S. Kumar, R. Baskaran, Identification of novel tyrosine kinase inhibitors for drug resistant T315l mutant BCR-ABL: a virtual screening and molecular dynamics simulations study, Sci. Rep. 4 (2014) 6948–6959. https://doi. org/10.1038/srep06948

[40] L.Z. Benet, C.M. Hosey, O. Ursu, T. I. Oprea, BDDCS, The rule of 5 and drugability, Adv. Drug. Deliv. Rev. 101 (2016) 89–98. https://doi.org/10.1016/j.addr.2016.05.007

Figure Captions

Fig. 1. Chemical structures of the investigated 1,3-diazaspiro[4.5]decane-2,4-diones (Series **1**, labeled as **1a**–**1i**), 1,3-diazaspiro[4.6]undecane-2,4-diones (Series **2**, labeled as **2a**–**2i**), and 5,5-diphenylhydantoins (Series **3**, labeled as **3a**–**3i**).

Fig. 2. The effect of he investigated compounds against proliferation of the HCT–116 cell line at concentration 100 μmol dm^{-3}. Data for the compounds **3a–3e** were taken from our previous paper [22].

Fig. 3. The effect of the investigated compounds against proliferation of the K562 cell line at concentration 100 μmol dm^{-3}.

Fig. 4. The effect of the investigated compounds against proliferation of the MDA–MB–231 cell line at concentration 100 μmol dm^{-3}. Data for the compounds **3a–3e** are taken from our previous paper [22].

Fig. 5. The asymmetric units of **1c** and **2a**. Displacement ellipsoids are drawn at 30% probability level and hydrogen atoms are shown as small spheres of arbitrary radii.

Fig. 6. The polymeric pseudo-chain of **1c** along the *b*-axis formed by hydrogen bonds (dashed lines). The hydrogen atoms are omitted for clarity.

Fig. 7. C–H$\cdots\pi$ interactions (dot lines) between adjacent chains in **1c.**

Fig. 8. The centrosymmetric dimer of **2a**. Symmetry code, (*i*): *–x*+1, *–y*, *–z*.

Fig. 9. The crystal packing diagram of **2a** in the almost *ac*-plane. Hydrogen bonds and C–H$\cdots\pi$ interactions are presented with dash and dot lines, respectively.

Fig. 10. The most stable conformations of compounds **1a** and **2a**.

Fig. 11. The absorption spectra of the compounds **2a**–**2g** at concentration ~1.0×10^{-5} mol dm^{-3} in ethanol.

Fig. 12. Relationships between ν_{max} and σ_p for the investigated 3-(4-substituted benzyl)-1,3-diazaspiro[4.6]undecane-2,4-diones (series **2**).

Fig. 13. Experimental (dashed line) and simulated (full line) UV-Vis absorption spectra of the compounds **2c** (a) and **2g** (b) in ethanol.

Fig. 14. The molecular orbitals and energy gaps between HOMO and LUMO of compounds **2a**, **2c**, **2g** and **2i** in the gas phase calculations.

Scheme 1. Synthesis of the investigated cyclohexanespiro-5-hydantoine derivatives (**1a**–**1g**) and cycloheptanespiro-5-hydantoine derivatives (**2a**–**2g**).

Scheme 2. Synthesis of the investigated cycloalkanespiro-5-hydantoine derivatives (**1h**, **1i, 2h**, **2i**) and 5,5-diphenylhydantoine derivatives (**3h**, **3i**).

Table 1. Crystal data and structure refinements for **1c** and **2a**.

Compound	**1c**	**2a**
Formula	$C_{16}H_{20}N_2O_3$	$C_{16}H_{20}N_2O_2$
Formula weight (g mol^{-1})	288.34	272.34
Crystal size (mm^3)	0.42×0.34×0.05	0.87×0.31×0.10
Crystal system	Monoclinic	Monoclinic
Space group	$P2_1/c$	$P2_1/n$
a (Å)	13.681(3)	12.783(3)
b (Å)	11.474(2)	6.2750(13)
c (Å)	10.089(2)	18.635(4)
β (°)	110.76(3)	105.94(3)
V (Å^3)	1480.9(5)	1437.3(5)
Z	4	4
F(000)	616	584
μ (mm^{-1})	0.090	0.084
ρ_c (g cm^{-3})	1.293	1.259
θ range (º)	3.18–25.35	3.32–26.02
Index ranges, h, k, l	–14→16 –7→13 –11→12	–15→15 –7→7 –23→23
R indices (all data)	0.0723[i]	0.0603[ii]
Goodness-of-fit	1.068	1.067
R_{int}	0.0221	0.0227
$\Delta\rho_{max}$, $\Delta\rho_{min}$ (e Å^{-3})	0.133, –0.193	0.292, –0.321

[i] $w = 1 / [s^2(F_o^2) + (0.0392P)^2 + 0.1715P]$ where $P = (F_o^2 + 2F_c^2)/3$;
[ii] $w = 1 / [s^2(F_o^2) + (0.1036P)^2 + 0.3109P]$ where $P = (F_o^2 + 2F_c^2)/3$.

Table 2. The experimental and calculated values of selected bond lengths, bond angles and torsion angles for compounds **1c** and **2a**.

Parameter	**1c** (exp.)	**1c** (calc.)	Parameter	**2a** (exp.)	**2a A** (calc.)[i]	**2a B** (calc.)[i]
Bond lengths (Å)			Bond length (Å)			
N1−C2	1.342(2)	1.367	N1−C2	1.337(2)	1.366	1.367
N1−C5	1.460(2)	1.466	N1−C5	1.455(2)	1.468	1.467
C2−O1	1.215(2)	1.212	C2−O1	1.224(2)	1.212	1.212
C2−N3	1.405(2)	1.413	C2−N3	1.391(2)	1.413	1.413
N3−C4	1.358(2)	1.375	N3−C4	1.369(2)	1.376	1.376
C4−O2	1.220(2)	1.212	C4−O2	1.206(2)	1.212	1.212
C4−C5	1.516(2)	1.539	C4−C5	1.526(2)	1.543	1.543
C5−C6	1.531(2)	1.543	C5−C6	1.539(3)	1.545	1.545
C5−C10	1.525(3)	1.546	C5−C11	1.527(3)	1.553	1.548
C6−C7	1.519(3)	1.534	C6−C7	1.506(3)	1.539	1.538
C7−C8	1.517(3)	1.535	C7−C8	1.508(5)	1.538	1.538
C8−C9	1.515(2)	1.535	C8−C9	1.482(4)	1.534	1.543
C9−C10	1.518(3)	1.535	C9−C10	1.510(3)	1.538	1.540
N3−C11	1.464(2)	1.468	C10−C11	1.520(3)	1.538	1.538
C11−C12	1.502(2)	1.513	N3−C12	1.447(2)	1.466	1.466
C12−C13	1.376(3)	1.394	C12−C13	1.509(3)	1.516	1.516
C12−C17	1.376(3)	1.402	C13−C14	1.377(3)	1.399	1.399
C13−C14	1.375(2)	1.396	C13−C18	1.379(3)	1.398	1.398
C14−C15	1.378(3)	1.397	C14−C15	1.379(3)	1.393	1.393
C15−C16	1.373(3)	1.400	C15−C16	1.367(3)	1.395	1.395
C16−C17	1.388(3)	1.387	C16−C17	1.372(3)	1.394	1.394
			C17−C18	1.389(3)	1.394	1.394
Bond angles (°)			Bond angles (°)			
N1−C5−C4	100.6(1)	100.7	N1−C5−C4	100.6(1)	100.3	100.4
N1−C5−C10	112.5(1)	112.5	N1−C5−C11	111.2(2)	109.7	111.4
C4−C5−C10	111.7(2)	110.0	C4−C5−C11	109.0(1)	109.5	108.7
N1−C5−C6	112.1(1)	112.4	N1−C5−C6	111.7(2)	112.3	112.2
C4−C5−C6	109.1(1)	110.3	C4−C5−C6	108.0(2)	108.8	108.0
C6−C5−C10	110.4(1)	110.6	C6−C5−C11	115.4(2)	115.1	114.9
Torsion angles (°)			Torsion angles (°)			
C4−N3−C11−C12	81.3(2)	91.8	C4−N3−C12−C13	–84.7(2)	−88.0	−86.0
N3−C11−C12−C13	–99.3(2)	–88.2	N3−C12−C13−C14	–11.3(2)	−85.2	−84.9
N1−C5−C6−C7	71.7(2)	72.8	N1−C5−C6−C7	65.9(2)	165.4	76.0
C4−C5−C6−C7	–177.6(2)	–175.8	C4−C5−C6−C7	175.6(2)	–85.4	−174.2
N3−C4−C5-C10	120.7(2)	121.7	N3−C4−C5−C11	119.1(2)	122.8	120.2
C2−N3−C11−C12	−102.3(2)	–88.1	C2−N3−C12−C13	101.0(2)	90.6	92.2

[i]Regarding the optimized conformations, the DFT calculations reveal two energetically close forms of **2a** (Fig. S1, Electronic Supplementary Information).

Table 3. The geometry of possible hydrogen bonds for compounds **1c** and **2a**.

Compound	D – H···A	d(D – H) (Å)	d(D···A) (Å)	d(H···A) (Å)	D – H···A (°)
1c	N1–H19···O2^{i}	0.846(1)	2.993(2)	2.149(1)	176(2)
	C18–H18A···O1^{ii}	0.960	3.608(3)	2.678	163
	C8–H8A···O1^{iii}	0.970	3.564(2)	2.682	151
	C7–H7B···O2^{i}	0.970	3.636(2)	2.763	150
	C9–H9A···O2^{i}	0.970	3.641(3)	2.772	149
	C10–H10B···O1^{iii}	0.970	3.640(2)	2.793	146
	C10–H10A···O2^{iv}	0.970	3.673(2)	2.842	144
2a	N1–H1···O1^{i}	0.860	2.928(2)	2.07	173
	C7–H7A···O1^{ii}	0.970	3.736(3)	2.772	173
	C7–H7B···O1^{i}	0.970	3.893(3)	2.943	167
	C10–H10B···O1^{i}	0.970	3.917(2)	2.975	164
	C11–H11A···O2^{iii}	0.970	3.472(2)	2.734	133

Symmetry codes: **1c**, (*i*): –*x*+1, *y*–1/2, –*z*+3/2; (*ii*): –*x*, *y*+1/2, –*z*+1/2; (*iii*): –*x*+1, *y*+1/2, –*z*+3/2; (*iv*): *x*, –*y*+1/2, *z*–1/2; **2a**, (*i*): –*x*, –*y*+1, –*z*+1; (*ii*): –*x*, –*y*, –*z*+1; (*iii*): –*x*+1/2, *y*+1/2, –*z*+3/2.

Table 4. UV-Vis spectral data for the compounds **2a**–**2g** in ethanol

Compound	**2a**	**2b**	**2c**	**2d**	**2e**	**2f**	**2g**
λ (nm)	208	211	225	220	220	229	266

Table 5. Calculated energies of the HOMO and LUMO orbitals and energy gap for compounds **1a**–**1i** and **2a**–**2i** in the gas phase and ethanol.

Compound	Gas phase			Ethanol		
	E_{HOMO} (eV)	E_{LUMO} (eV)	E_{gap} (eV)	E_{HOMO} (eV)	E_{LUMO} (eV)	E_{gap} (eV)
1a	−6.98	−0.69	6.26	−7.13	−0.84	6.29
1b	−6.67	−0.63	6.04	−6.81	−0.74	6.07
1c	−6.19	−0.59	5.60	−6.37	−0.74	5.63
1d	−6.90	−0.91	5.99	−7.03	−0.99	6.04
1e	−6.83	−0.95	5.88	−6.95	−1.02	5.93
1f	−7.45	−1.84	5.61	−7.41	−1.83	5.58
1g	−7.68	−2.86	4.82	−7.49	−3.10	4.39
1h	−7.33	−2.16	5.17	−7.44	−2.22	5.21
1i	−7.34	−2.29	5.05	−7.39	−2.34	5.05
2a	–6.97	–0.64	6.33	–7.09	–0.76	6.31
2b	–6.68	–0.58	6.09	–6.81	–0.69	6.12
2c	–6.20	–0.55	5.66	–6.37	–0.70	5.67
2d	–6.91	–0.91	6.00	–7.02	–0.99	6.03
2e	–6.83	–0.95	5.89	–6.96	–1.02	5.93
2f	–7.44	–1.84	5.60	–7.42	–1.87	5.54
2g	–7.65	–2.86	4.79	–7.48	–3.13	4.35
2h	–7.33	–2.18	5.15	–7.43	–2.22	5.21
2i	–7.34	–2.31	5.03	–7.39	–2.34	5.05

Table 6. Lipinski parameters of the investigated compounds

Compound	Molecular weight (g mol^{-1})	*C*log *P* [i]	Hydrogen bonds		Rotatable bonds	Polar surface area[iv] ($Å^2$)	Violations
			Donors[ii]	Acceptors[iii]			
1a	258.32	2.79	1	4	2	74.50	0
1b	272.35	3.07	1	4	2	73.70	0
1c	288.35	2.51	1	5	3	94.40	0
1d	292.77	3.35	1	4	2	77.80	0
1e	337.22	3.62	1	4	2	76.90	0
1f	283.33	2.93	1	5	2	135.9	0
1g	303.32	2.82	1	7	3	167.7	1
1h	304.32	2.13	1	5	3	110.00	0
1i	320.78	2.53	1	5	3	110.00	0
2a	272.35	3.21	1	4	2	74.60	0
2b	286.38	3.49	1	4	2	77.70	0
2c	302.37	2.93	1	5	3	93.10	0
2d	306.79	3.77	1	4	2	75.30	0
2e	351.24	4.04	1	4	2	77.10	0
2f	297.36	3.35	1	5	2	129.8	0
2g	317.35	3.24	1	7	3	169.2	1
2h	318.35	2.55	1	5	3	107.7	0
2i	334.80	2.95	1	5	3	108.5	0
3a[iv]	342.40	4.41	1	4	4	69.26	0
3b[iv]	356.43	4.69	1	4	4	68.17	0
3c[iv]	372.42	4.13	1	5	5	85.08	0
3d[iv]	376.84	4.97	1	4	4	68.61	0
3e[iv]	421.29	5.24	1	4	4	68.97	1
3f[iv]	367.41	4.55	1	5	4	124.9	0
3g[iv]	387.39	4.45	1	7	5	161.9	1
3h[iv]	388.40	3.76	1	5	5	100.6	0
3i[iv]	404.85	4.16	1	5	5	99.90	0
Ideal compound [27]	< 500	< 5	< 5	< 10	< 8	< 140	≤ 1

[i]Calculated with B3LYP\6-311++G(d,p);
[ii]A donor indicates any OH or NH groups;
[iii]An acceptor indicates any O or N including those in donor groups;
[iv]Taken from our previous study [22].

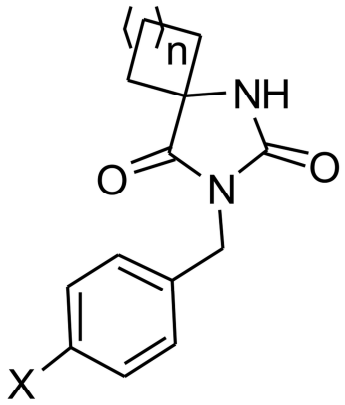

Compound	n	X
1a	3	H
1b	3	CH_3
1c	3	CH_3O
1d	3	Cl
1e	3	Br
1f	3	CN
1g	3	NO_2
2a	4	H
2b	4	CH_3
2c	4	CH_3O
2d	4	Cl
2e	4	Br
2f	4	CN
2g	4	NO_2

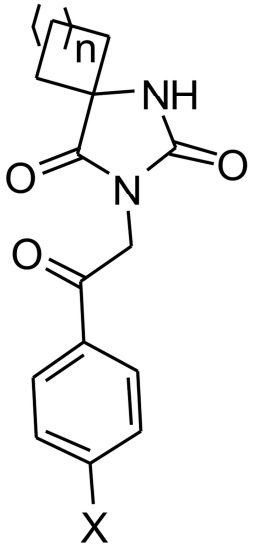

Compound	n	X
1h	3	F
1i	3	Cl
2h	4	F
2i	4	Cl

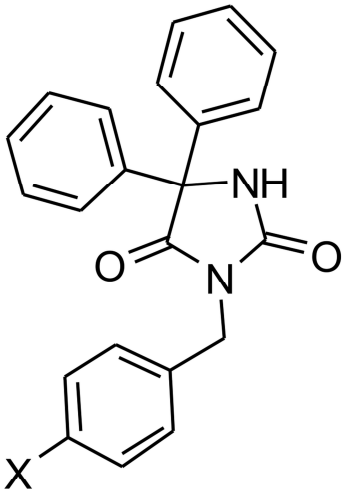

Compound [22]	X
3a	H
3b	CH_3
3c	CH_3O
3d	Cl
3e	Br
3f	CN
3g	NO_2

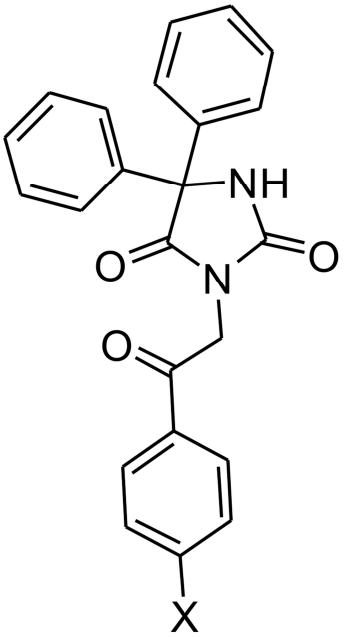

Compound [21]	X
3h	F
3i	Cl

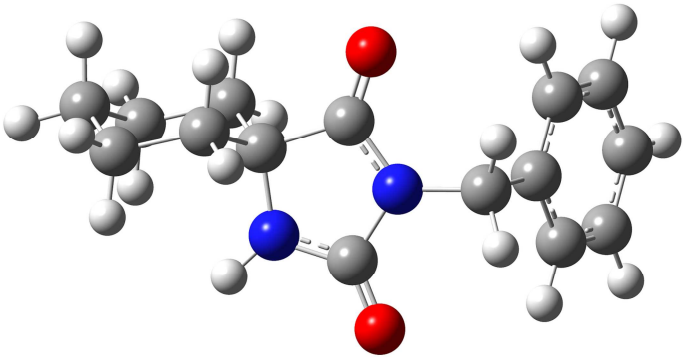

1a

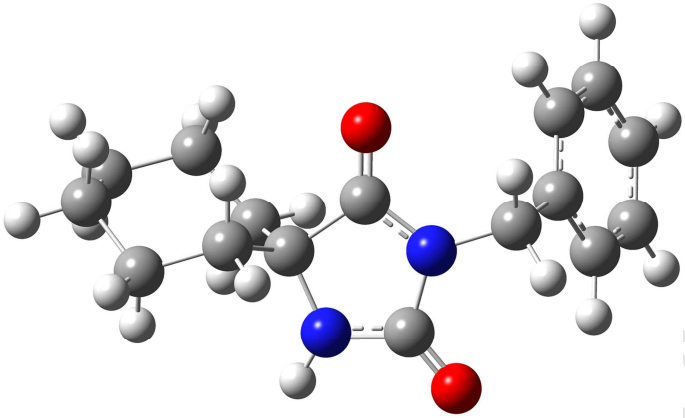

2a

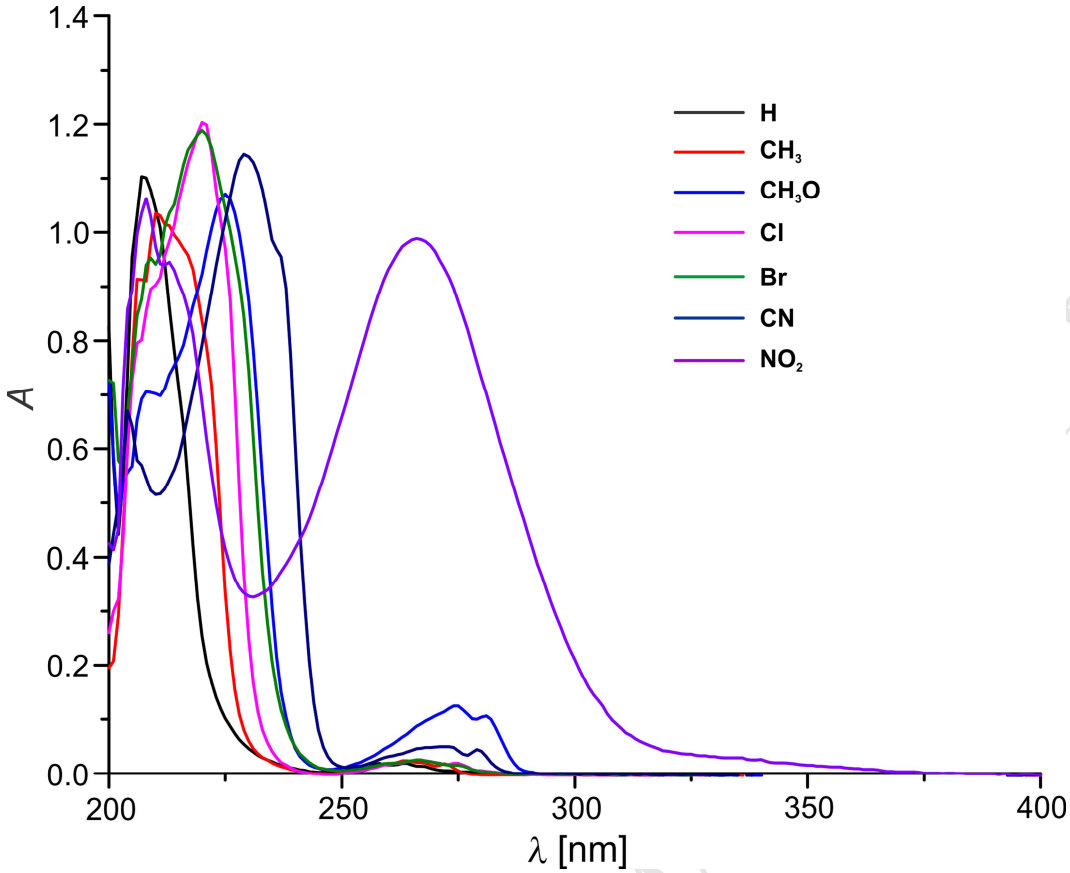

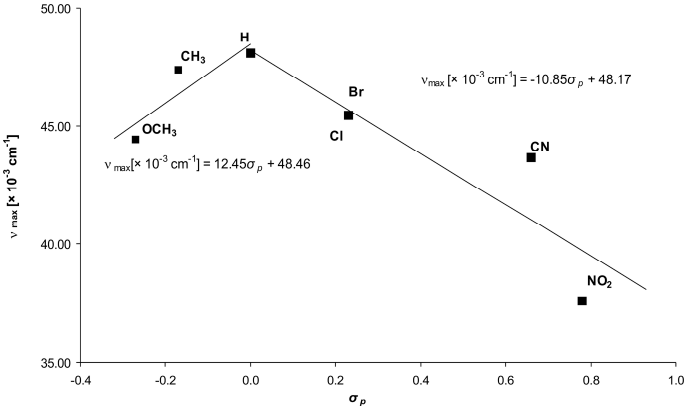

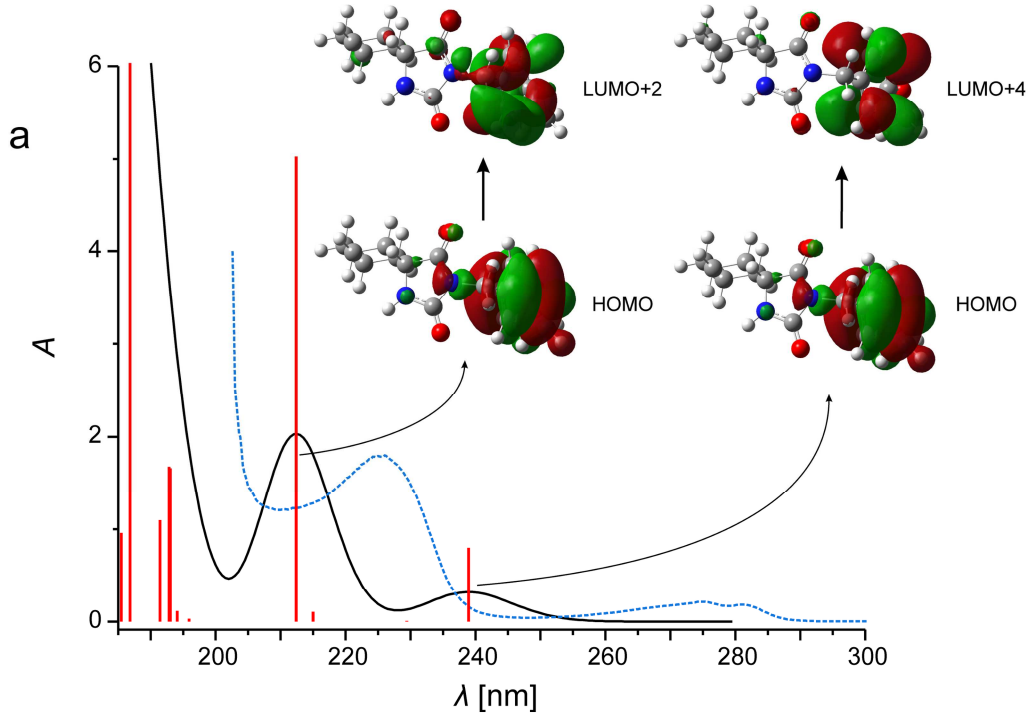
a
LUMO+2
LUMO+4
HOMO
HOMO
A
λ [nm]

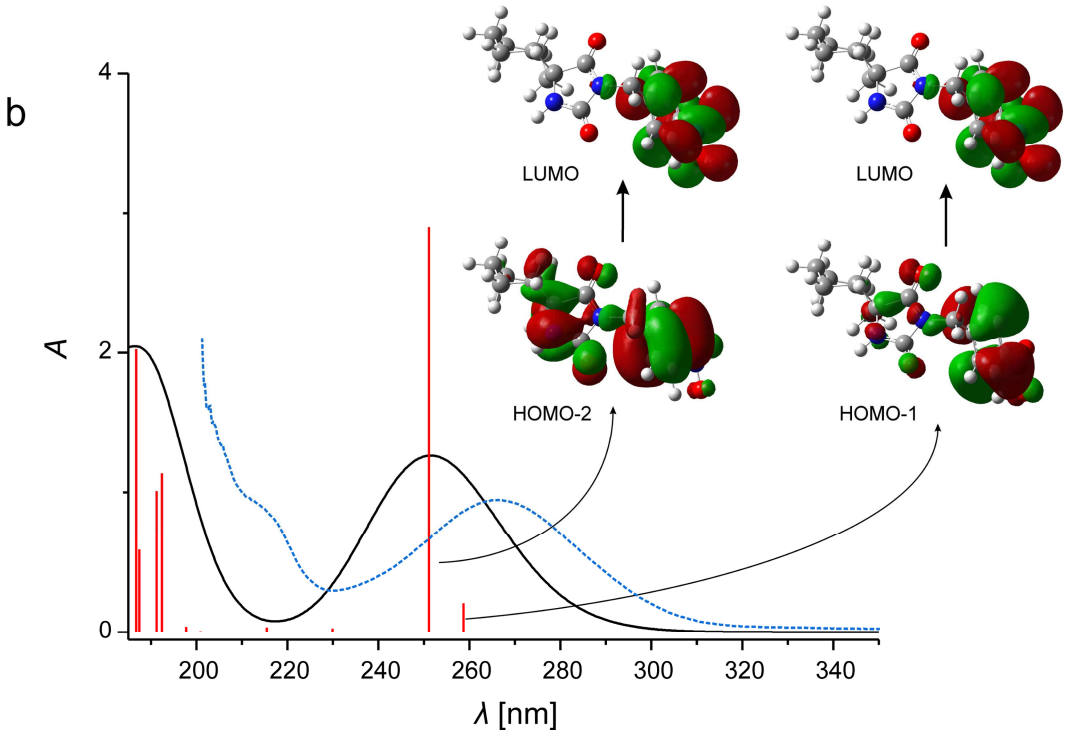
b
LUMO
LUMO
HOMO-2
HOMO-1
A
λ [nm]

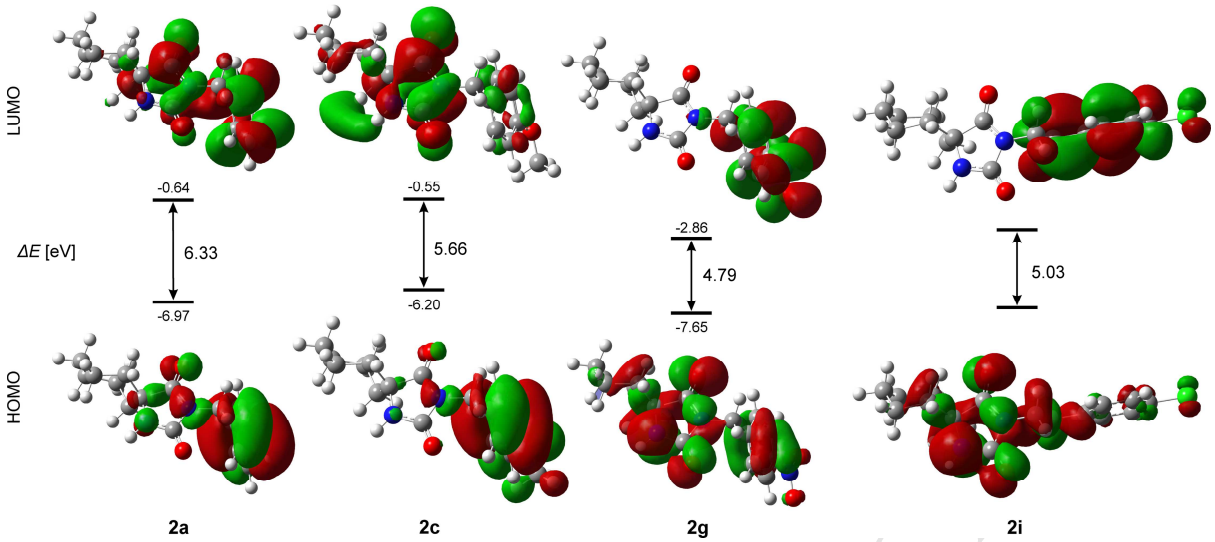

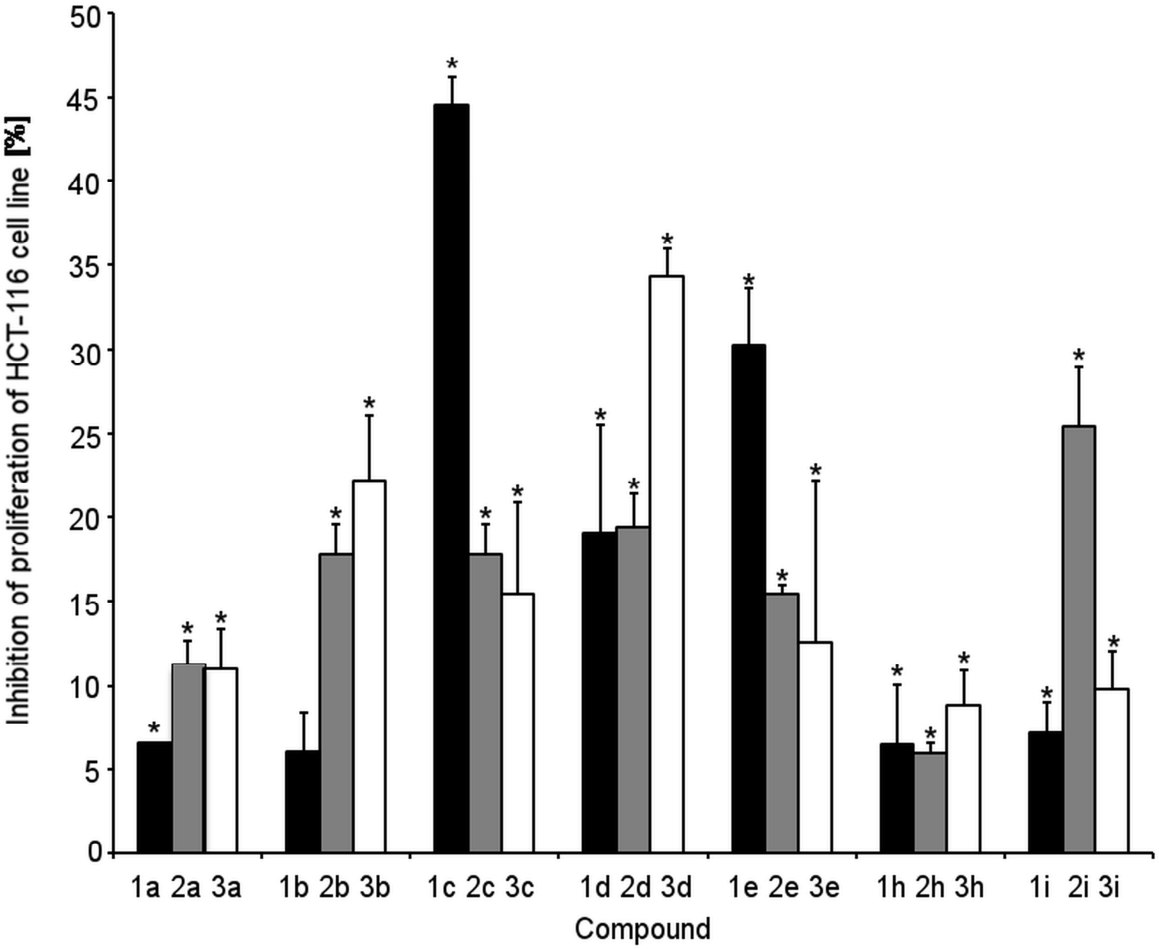
Inhibition of proliferation of HCT-116 cell line [%]
50
45
40
35
30
25
20
15
10
5
0
1a 2a 3a
1b 2b 3b
1c 2c 3c
1d 2d 3d
1e 2e 3e
1h 2h 3h
1i 2i 3i
Compound

I

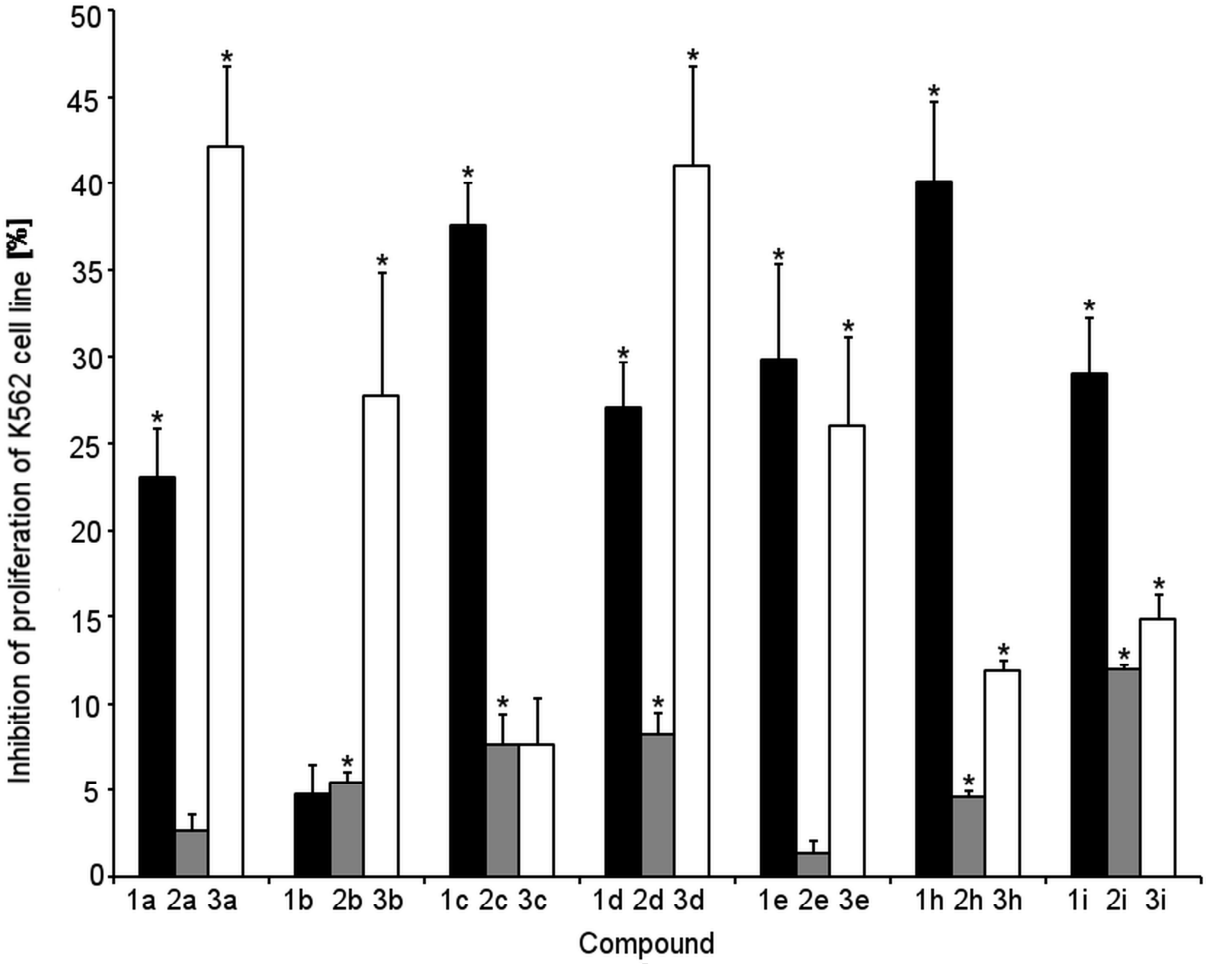
Inhibition of proliferation of K562 cell line [%]
50
45
40
35
30
25
20
15
10
5
0
1a 2a 3a
1b 2b 3b
1c 2c 3c
1d 2d 3d
1e 2e 3e
1h 2h 3h
1i 2i 3i
Compound

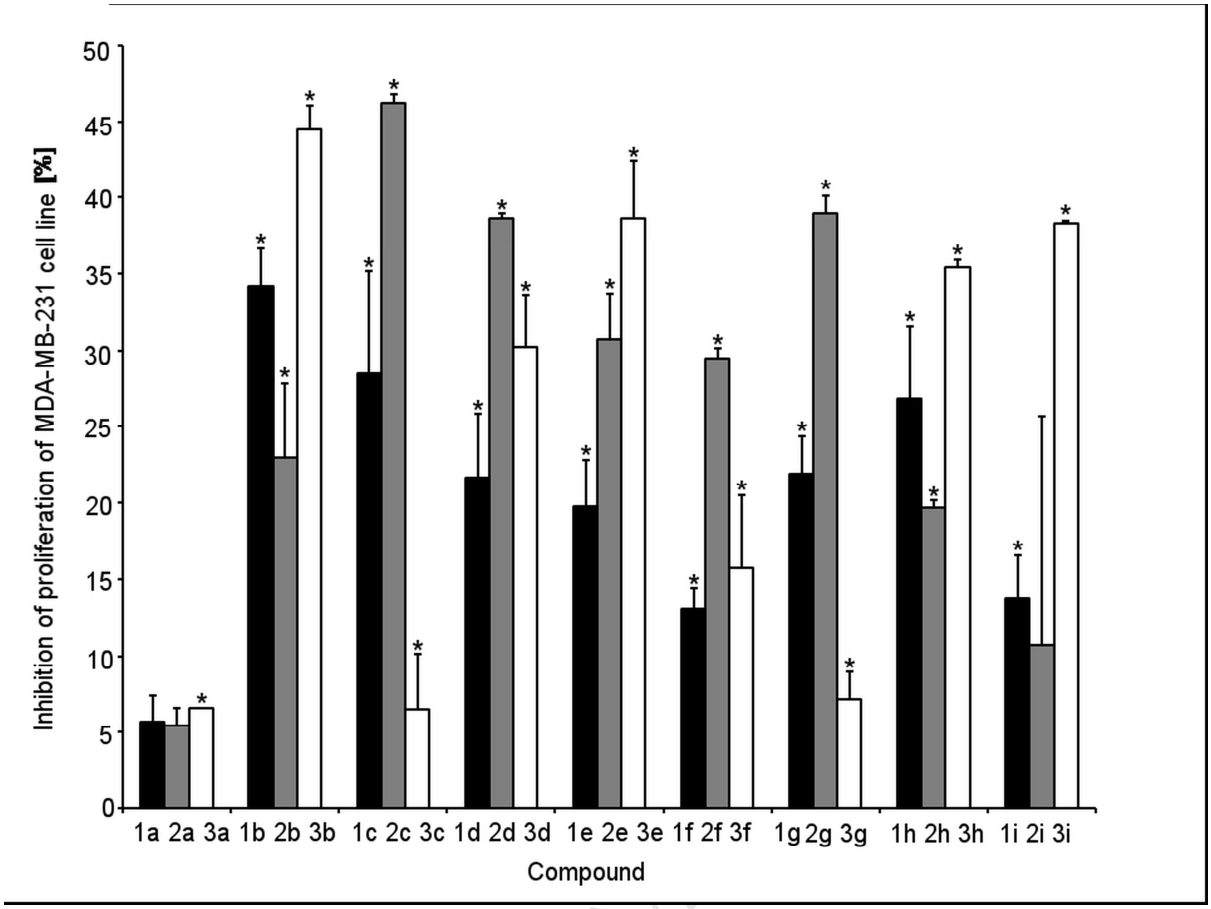

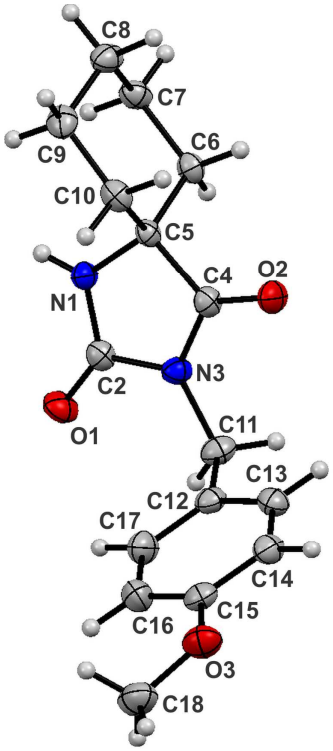

1c

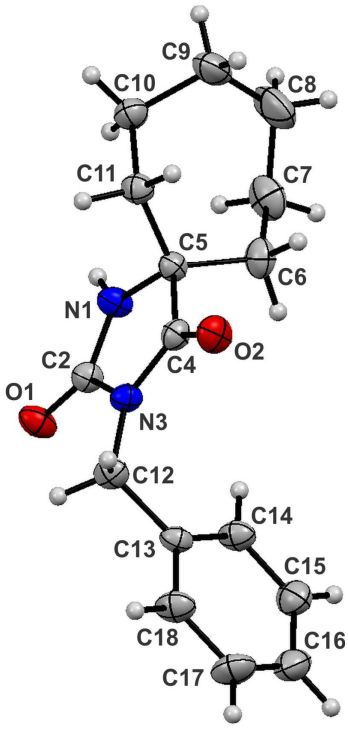

2a

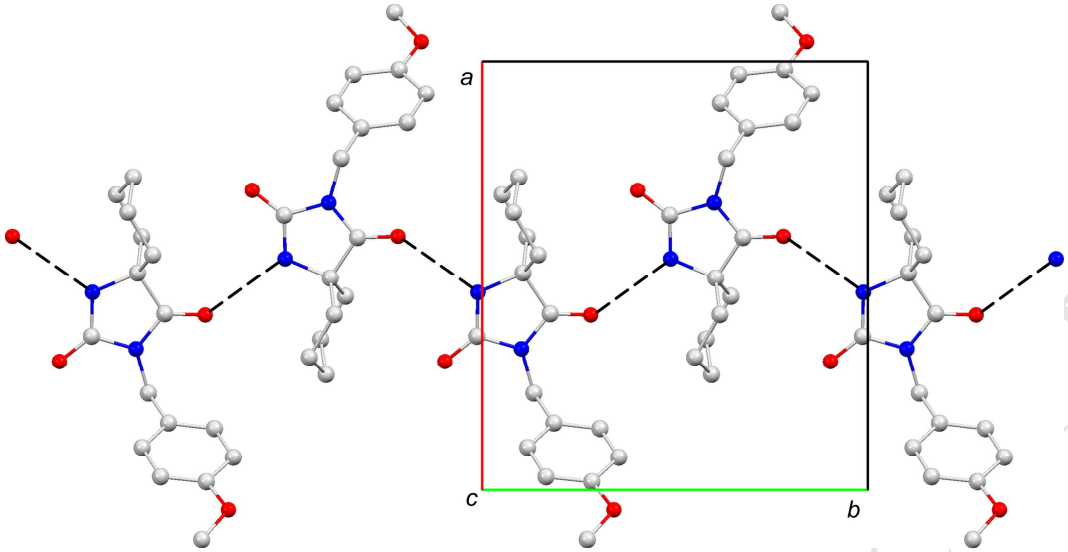

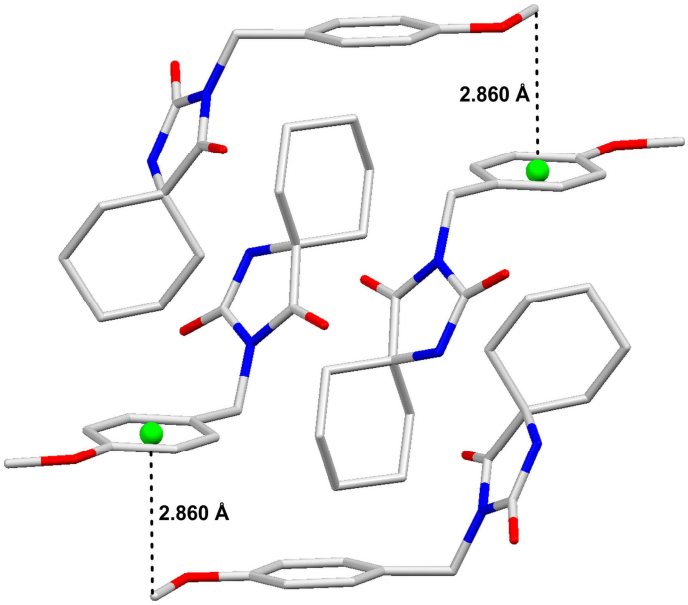

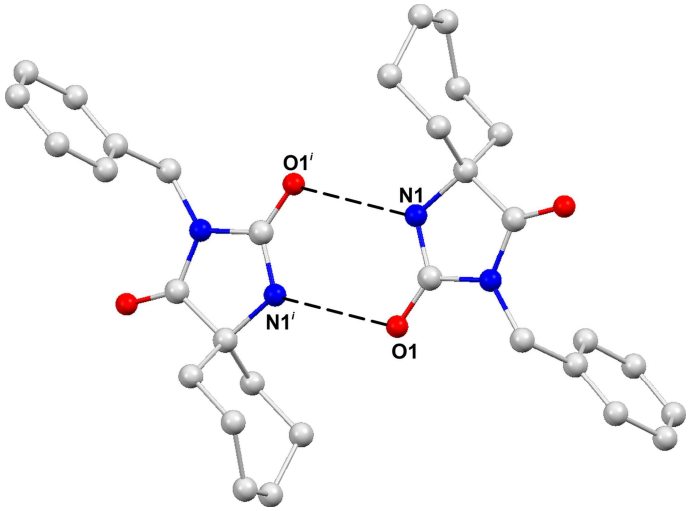

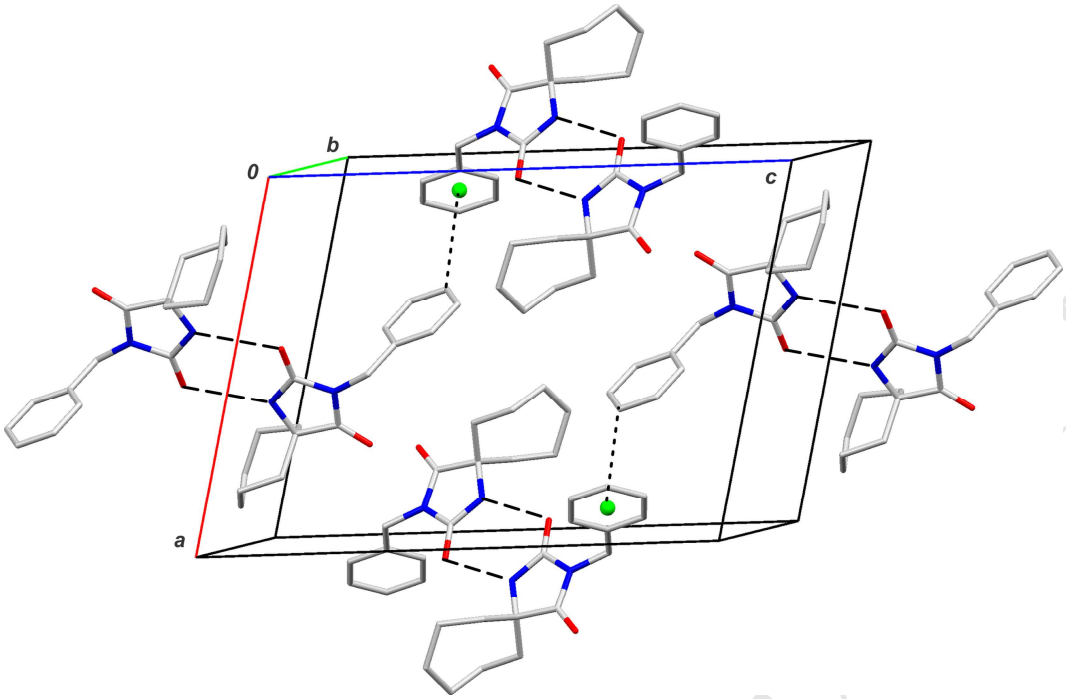

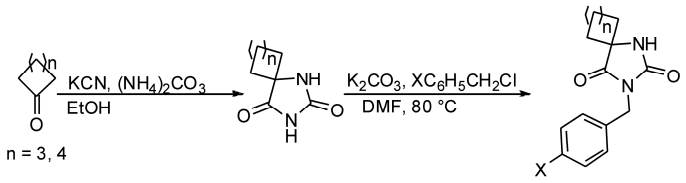

n = 3, 4

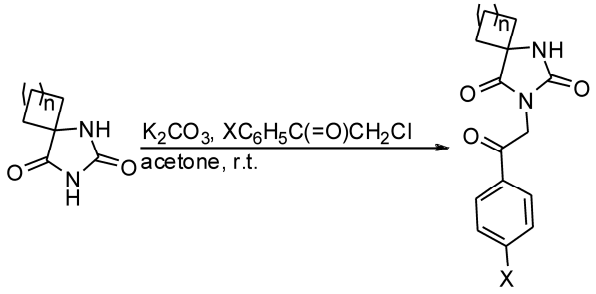

1h, 1i, 2h, 2i

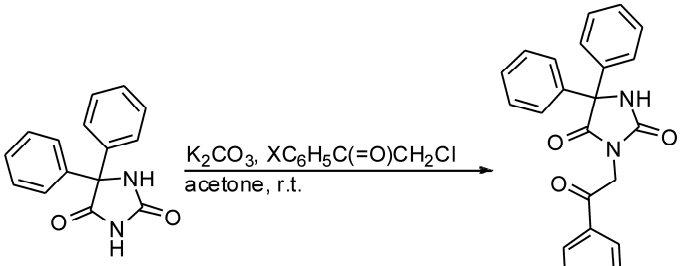

3h, 3i

Highlights

1. In searching for new hydantoin-based drugs, two series of compounds were synthesized.
2. Compounds with the CH_3O, Cl or Br group exhibited an improved antiproliferative activity.
3. Different modes of intermolecular aggregation in the crystal structures were identified.
4. Substituent effects were reflected in the geometries and electronic structures.
5. The investigated compounds were compatible with the Lipinski rule of five.